PNAS
www.pnas.org

Supplementary Information for

Monovalent ions modulate the flux through multiple folding pathways of an RNA pseudoknot

Jorjethe Roca[a,1], Naoto Hori[b], Saroj Baral[a], Yogambigai Velmurugu[a,2], Ranjani Narayanan[a,3], Prasanth Narayanan[a], D. Thirumalai[b], and Anjum Ansari[a,c,4]

[a]Department of Physics and [c]Department of Bioengineering,

University of Illinois at Chicago, Chicago, IL 60607

[b]Department of Chemistry, University of Texas at Austin, Austin, TX 78712

[1]Present address: Thomas C. Jenkins Department of Biophysics, Johns Hopkins University, Baltimore, MD 21218

[2]Present address: Laura and Isaac Perlmutter Cancer Center and Department of Pathology, New York University School of Medicine, New York, NY 10016

[3]Present address: Division of Physics & Applied Physics, School of Physical and Mathematical Sciences, Nanyang Technological University, Singapore 637371

[4]Corresponding author: Anjum Ansari (E-mail: ansari@uic.edu)

This PDF file includes:

Supplementary text: SI Methods 1.1-1.10
Figures S1 to S16
Tables S1 to S8
References for SI reference citations

www.pnas.org/cgi/doi/10.1073/pnas.1717582115

Supplementary Information Text

SI Methods

1.1 RNA samples. Unlabeled RNA samples were obtained from Dharmacon Inc., CO. 2-aminopurine (2AP) and pyrrolocytidine (pC) labeled samples were obtained from TriLink Biotechnologies, CA. In this study, three RNA constructs were used: the pseudoknot VPK and its constituent hairpins HP1 and HP2 (Figure 1). The pseudoknot samples were either unlabeled, labeled with 2AP at position 20 (VPK-2AP), or labeled with pC at position 31 (VPK-pC). Similarly, the constituent hairpins were either unlabeled, or labeled with 2AP at the same position as in VPK-2AP (HP1-2AP), or labeled with pC at the same position as in VPK-pC (HP2-pC). All pseudoknot and hairpin samples were purchased with PAGE purification. Two short oligonucleotides, 2AP-ref (5'-CC[2AP]CU-3') and pC-ref (5'-GC[pC]CA-3'), were used as reference samples to measure the temperature dependence of the quantum yield of the 2AP and pC probes, respectively, in a sequence context identical to that in the VPK or the constituent hairpins. The reference samples were purchased with HPLC purification. Strand concentrations for all measurements were calculated by making absorbance measurements at 260 nm, with extinction coefficients of 323,500 $M^{-1}cm^{-1}$ for VPK; 325,100 $M^{-1}cm^{-1}$ for VPK-2AP and VPK-pC; 176,000 $M^{-1}cm^{-1}$ for HP1; 247,700 $M^{-1}cm^{-1}$ for HP2; 212,700 $M^{-1}cm^{-1}$ for HP1-2AP; and 248,900 $M^{-1}cm^{-1}$ for HP2-pC; as reported by the manufacturer.

All measurements were made in 10 mM 3-(N-morpholino) propanesulfonic acid (MOPS) buffer pH 7.0, with either 50 mM KCl or a range of NaCl concentrations from 100 mM to 1 M. Prior to measurements, the samples were unfolded by first heating to 60 °C and waiting at that temperature for 10 minutes, then further heating to 90 °C and waiting there for 10 more minutes followed by cooling on ice and equilibration for another 10 minutes.

1.2 Equilibrium melting experiments. Absorbance melting profiles were collected using a UV-Vis spectrophotometer Cary50 (Varian Instruments, CA). The sample absorbance was measured in a quartz cuvette of 1 or 0.1 cm path length, with excitation at 260 nm. The temperature of the sample cuvette was controlled by a Peltier device incorporated in the instrument. Melting profiles were obtained by making absorbance

measurements as a function of temperature, with the temperature increased at a rate of 0.4 °C/min from 20 °C to 91 °C, in steps of 1 °C. Reversibility was checked by cooling the sample back to its initial temperature and immediately repeating the melting measurements.

Fluorescence equilibrium melting profiles were obtained using a Fluoromax-4 (HORIBA Instruments Inc., NJ) spectrofluorimeter. 2AP- (pC-) labeled samples were excited at 310 (350) nm and the fluorescence emission spectra collected over a wavelength range of 320 nm – 600 nm (360 nm – 600 nm). Fluorescence emission spectra were recorded every 2 °C from 15 °C to 93 °C after an equilibration time of 5 min at each temperature. The melting profiles were constructed by plotting the maximum of the fluorescence emission spectra (at 370 nm for 2AP-labeled samples and at 460 nm for pC-labeled samples) for each measurement versus temperature. Reversibility was checked as described above.

All absorbance or fluorescence melting profiles were smoothed (over 5 points) using the moving average option of the smooth built-in function of MATLAB (R2014a 8.3.0.532). The individual (smoothed) melting profiles for each sample (2-3 per set of conditions) were averaged together prior to analysis; the uncertainties in the data were calculated as the standard error of the mean (SEM). For clarity, only every other data point is shown in the melting profile figures in the manuscript.

The discretized derivatives of the absorbance and fluorescence melting profiles, $\delta A/\delta T$ and $\delta F/\delta T$, respectively, were calculated by computing the difference between adjacent points for each of the melting profiles after they were normalized at 20 °C. The derivative profiles from the individual experiments were subsequently further smoothed (over 5 points) and averaged; the uncertainties reported are the corresponding SEM, as described above.

1.3 Analysis of the equilibrium melting profiles. Equilibrium melting profiles of all hairpins were fitted in terms of a two-state system: HP ⇔ U, with HP denoting the folded (hairpin) state and U the unfolded state. The melting profiles for the VPK pseudoknot were described in terms of either a three-state-system (e.g. melting profiles at 50 mM KCl): PK ⇔ pkHP ⇔ U, with PK the fully folded state and pkHP a partially folded hairpin intermediate; or in terms of a four-state system (e.g. melting profiles at 100 mM to 1 M

NaCl) with parallel folding pathways that populated two partially folded hairpin intermediates pkHP1 and pkHP2, as illustrated in Figure 3.

The equilibrium populations of the different macrostates in any of the above kinetic schemes were described as a function of temperature in terms of the free energy difference ΔG_{io} between the *i*-th macrostate and a reference state (typically chosen as the most folded state) as follows:

$$P_{i_{eq}}(T) = \frac{\exp\left(-\frac{\Delta G_{io}}{RT}\right)}{\sum_i \exp\left(-\frac{\Delta G_{io}}{RT}\right)} \tag{S1}$$

For macrostates not directly connected to the reference state, for example macrostate *j* in the three-state system: o $\Leftrightarrow i \Leftrightarrow j$, ΔG_{jo} was written as the sum of the free energy differences between the *j*-th and *i*-th states (ΔG_{ji}) and ΔG_{io} as:

$$\Delta G_{jo}(T) = \Delta G_{ji}(T) + \Delta G_{io}(T) \tag{S2}$$

Furthermore, ΔG_{ji} was parameterized in terms of two parameters, the enthalpy change ΔH_{ji} and a transition or "melting" temperature T_{mji}, defined as the temperature at which the *i*-th and *j*-th macrostate are equally populated (i.e. the temperature at which $\Delta G_{ji} = 0$). Thus,

$$\Delta G_{ji}(T) = \Delta H_{ji}\left(1 - \frac{T}{T_{mji}}\right) \tag{S3}$$

The equilibrium fluorescence (or absorbance) intensity measured as a function of temperature was written as:

$$F_{eq}(T) = \sum_i F_i(T) P_{i_{eq}}(T) \tag{S4}$$

where $F_i(T)$ was the fluorescence (or absorbance) level of the molecule in the *i*-th macrostate at temperature *T*. We further parameterized $F_i(T)$ as a linear function in temperature:

$$F_i(T) = F_{io}\left[m_i\left(T - T_0^{eq}\right) + 1\right] \tag{S5}$$

The parameter F_{io} in Eq. S5 describes the fluorescence (or absorbance) level of the *i*-th macrostate at a reference temperature T_0^{eq} and m_i is the corresponding slope describing the temperature dependence of $F_i(T)$. The reference temperature for all equilibrium measurements was fixed at $T_0^{eq} = 20$ °C.

For the absorbance melting profiles, all baselines were constrained to have the same slope. For the fluorescence melting profiles, this constraint was relaxed, although the baselines corresponding to the completely unfolded state were constrained to have the same slope as the fluorescence profiles for the reference samples 2AP-ref or pC-ref at each salt. Additional constraints imposed on the thermodynamic and baseline parameters when fitting the VPK-2AP and VPK-pC melting profiles as a function of different salt conditions are described in SI Methods 1.4.

The thermodynamic and baseline parameters needed to describe the melting profiles were obtained by fitting either the melting profiles directly (Method 1) or by fitting the derivative profiles (Method 2). The derivative of the melting profiles $\partial F/\partial T$ can be obtained numerically from the measured $F(T)$ as:

$$\frac{\partial F}{\partial T} = \sum_i \left[\frac{\partial F_i}{\partial T} P_{ieq}(T) + F_i(T) \frac{\partial P_{ieq}}{\partial T}\right] \tag{S6}$$

with the derivative of the fluorescence of the *i*-th microstate parametrized as:

$$\frac{\partial F_i}{\partial T} = F_{io} m_i \tag{S7}$$

and:

$$\frac{\partial P_{ieq}}{\partial T} = \frac{1}{RT} \frac{\exp\left(-\frac{\Delta G_{io}}{RT}\right)}{\sum_i \exp\left(-\frac{\Delta G_{io}}{RT}\right)} \left\{ \frac{\Delta G_{io}}{T} - \frac{\partial \Delta G_{io}}{\partial T} - \frac{1}{RT} \frac{\sum_i \left[\exp\left(-\frac{\Delta G_{io}}{RT}\right)\left(\frac{\Delta G_{io}}{T} - \frac{\partial \Delta G_{io}}{\partial T}\right)\right]}{\sum_i \exp\left(-\frac{\Delta G_{io}}{RT}\right)} \right\} \tag{S8}$$

As an example, for the case of a three-state system o ⇔ i ⇔ j, $\partial \Delta G_{jo}/\partial T$ for the *j*-th macrostate is:

$$\frac{\partial \Delta G_{jo}}{\partial T} = \frac{\partial \Delta G_{ji}}{\partial T} + \frac{\partial \Delta G_{io}}{\partial T} \tag{S9}$$

with the derivative of the free energy difference between two states written in terms of the parameters ΔH_{ji} and T_{mji}:

$$\frac{\partial \Delta G_{ji}}{\partial T} = -\frac{\Delta H_{ji}}{T_{mji}} \tag{S10}$$

For both methods, the melting parameters were obtained by fitting the absorbance or fluorescence melting profiles (or their derivatives) as a function of temperature using a least-square non-linear procedure in MATLAB (R2014A 8.3.0.532) that minimized the chi-square χ^2 (1):

$$\chi^2 = \sum_{i=1}^{N} \frac{1}{\sigma_i^2} \left\{ \left(F_i - F(T_i) \right)^2 \right\} \quad \text{(S11)}$$

where σ_i is the uncertainty (SEM) associated with the *i*-th data point.

The thermodynamic parameters that described the transitions between different macrostates of the system (ΔH_{ji} and T_{mji} for each transition $i \Leftrightarrow j$) for the different samples are summarized in SI Tables S1–S6. The primary source of error in the fitting parameters, estimated as described in SI Methods 1.5, is from incomplete information about the temperature dependence of the linear baselines. We note that the number of parameters needed to describe the melting profiles increases rapidly as the number of macrostates increases. For example, for a three-state system with unconstrained baselines, the total number of parameters are 10 (6 parameters for the three baselines and 4 parameters needed to describe two free energy differences at all temperatures). If all baselines are constrained to have the same slopes, as in the absorbance measurements, the total number of parameters is 8 (4 for the baselines and 4 for the free energy parameters). For a four-state system with unconstrained baselines, the number of parameters increase to 14 (8 for the baselines and 6 for the free energy differences). Our VPK melting profiles do not have sufficient information to obtain these parameters independently, especially in the case of the 4-state parallel pathway scheme needed to describe the salt dependence of VPK-2AP and VPK-pC melting data. Therefore, to limit the number of free parameters, we imposed additional constraints from either other experiments or from simulations, as described below.

1.4 Analysis of the VPK-2AP and VPK-pC equilibrium melting profiles as a function of salt. For VPK-2AP measurements in 50 mM salt, we assumed that only one unfolding pathway via pkHP1 was the dominant pathway and used the three-state sequential pathway scheme to describe the melting profiles; at higher salt, we used the four-state parallel pathway scheme with the following constraints on the baseline parameters:

the fluorescence levels for pkHP2 were assumed to be the same as those for U, and the slopes of all the U baselines at each salt condition were fixed from the slopes of the corresponding 2AP-ref measurements (SI Figure S3*A*). We further constrained the ΔH and T_m parameters for the pkHP1 ⇔ U transition at each salt from the corresponding parameters for the unfolding of the hairpins HP1-2AP (from fluorescence measurements, SI Figure S4) and for the pkHP2 ⇔ U transition from the unfolding of HP2 (from absorbance measurements, SI Figure S9). Furthermore, we carried out two sets of fits in which we constrained the T_m for either the PK ⇔ pkHP1 or the PK ⇔ pkHP2 transition at each salt to be within 5 °C of the values predicted by the simulations, as described in SI methods 1.10. Note that with constraints on 3 of the 4 transitions imposed by either experiments on hairpins or simulations, the thermodynamic parameters for the 4th transition are determined from thermodynamic linkage. We also clarify that all constraints, unless otherwise noted, allowed that parameter to vary within 10% of its constrained value.

Similarly, for VPK-pC melting profiles at 50 mM KCl, we assumed a single dominant pathway via pkHP1, and a four-state parallel pathway at higher salt. In the four-state fits, the baselines for PK and pkHP2 (both with pC context in the structured stem 2) were assumed identical; the baselines for pkHP1 and U (both with pC context in an unstructured single-strand) were assumed identical; the slope of the unfolded (U) baseline was constrained to be the same at all salt conditions, as guided by our measurements on pC-ref that exhibited no salt dependence in the thermal profiles (SI Figure S3*B*). The ΔH and T_m parameters for the pkHP1 ⇔ U transition were constrained from the corresponding parameters for the unfolding of the hairpin HP1 (from absorbance measurements, SI Figure S8). The ΔH and T_m parameters for the pkHP2 ⇔ U transition were constrained from the corresponding parameters for the unfolding of the HP2-pC hairpin as probed by pC fluorescence (SI Figure S11), with the exception of the parameters at 1 M NaCl, since they were not well determined by the HP2-pC fluorescence melting profile. Instead, for 1 M NaCl, the parameters were given a broader range with the constraint that the T_m for the pkHP2 ⇔ U transition was constrained to be higher than that at 500 mM NaCl. Finally, as in VPK-2AP, the T_m for either the PK ⇔ pkHP1 or the PK ⇔ pkHP2 transition was constrained to be within 5 °C of the values predicted by the simulations.

1.5 Error estimation of melting parameters. To obtain the uncertainties in the thermodynamic parameters needed to fit the melting profiles, we fixed each fitting parameter at different values over some range in the vicinity of its optimal value and refitted the melting data by allowing the rest of the parameters to vary and to minimize the χ^2. From the χ^2 versus parameter value plots thus generated (SI Figure S2), the uncertainties in the parameters were identified as the values at which χ^2 changes by 1; this increase: $\Delta\chi^2 = 1$ corresponds to one standard deviation in parameter space (1). The lower and upper errors in the parameters are represented as sub and superscripts in the SI Tables.

1.6 Temperature jump experiments. Kinetic measurements were carried out using a home-built laser temperature jump (T-jump) apparatus, which uses 10-ns laser pulses at 1550 nm, generated by Raman shifting the 1064 nm pulses from the output of an neodymium-doped yttrium aluminum garnet (Nd:YAG) laser, to rapidly heat a small volume of the sample within ~10 ns (2, 3). The laser pulses were focused to ~1 mm spot size onto a 2-mm wide sample cuvette of path length 0.5 mm. Each laser pulse (~40 mJ/pulse at the sample position) yielded ~3–10 °C T-jump at the center of the heated volume. Kinetics traces were measured only for the 2AP-labeled samples (HP1-2AP and VPK-2AP). The probe source for excitation of 2AP was a 200-W Hg–Xe lamp, with the excitation wavelengths selected by a broadband filter centered at 320 nm (BrightLine 320/40, Semrock, Rochester, New York). The fluorescence emission intensity was monitored using a Hamamatsu R928 photomultiplier tube equipped with another broadband filter (BrightLine 370/36, Semrock, Rochester, New York) and coupled with a preamplifier Hamamatsu C1053-51 and recorded in a 500 MHz transient digitizer (Tektronix, DPO4054B, Beaverton, OR).

The initial temperature of the sample was measured using a thermistor (YSI 44008; YSI Inc., Yellow Springs, OH) in direct contact with the sample cell. The magnitude of the temperature change upon T-jump perturbation was determined from measurements on control (2AP-ref) samples, for which no relaxation kinetics other than T-jump recovery are expected (see SI Figure S5), as described in SI Methods 1.8. The errors in the T-jump estimates are about 10–20%.

1.7 Acquisition and analyses of T-jump relaxation traces. To acquire data with the highest temporal resolution and be able to span several orders of magnitudes in time scale, it is necessary to measure T-jump kinetics traces over different time scales and then combine these traces. We typically acquired the kinetics traces on at least two time scales, with one million data points in each trace; the short time scale covered kinetics up to 2 ms, with a time-resolution of 2 ns, while the longer time scale covered kinetics up to 400 ms, with a time-resolution of 400 ns. For each time scale, 512 kinetics traces were acquired and averaged by the digitizer and saved for further analysis. The data acquired in the short time scale were reduced to 400 points and the data in the long time scale were reduced to 2,000; in both cases a logarithmic average approach was used. In this approach, the temporal data was converted to a logarithmic scale and a given amount of points were averaged together to yield only 100 points per logarithmic decade. Given that there are more data points in time decades corresponding to longer times, the number of points averaged increased as the time increased. By averaging this way, the resolution in the smallest time scale is preserved while the high density of points in the highest time scale is reduced. Prior to any further analysis, data acquired below ~30 μs in each trace were discarded because of artifacts either from scattered infrared laser light into the photomultiplier tube, or due to cavitation effects from microbubbles in the samples (4).

In order to combine the data acquired over the two different time scales, the two traces were fitted simultaneously with a double-exponential decay convoluted with T-jump recovery kinetics, with an additional multiplicative factor applied to one of the traces to account for any systematic difference in the measured intensities for the two traces. The double-exponential decay with T-jump recovery is described by:

$$I(t) = \{[I(0^+) - I_1]\exp(-k_1 t) + [I_1 - I(\infty)]\exp(-k_2 t) - I(0^-)\} f_{rec}(t) + I(0^-) \quad \text{(S12)}$$

Here, k_1 and k_2 are the two relaxation rates, $I(0^-)$ is the intensity at the initial temperature, $I(0^+)$ is the intensity immediately after the T-jump, I_1 is the intensity at the end of the fast relaxation process, $I(\infty)$ is the intensity at the end of both relaxation processes, and $f_{rec}(t) = (1 + t/\tau_{rec})^{-1}$ describes the time-dependence of the decay of the T-jump itself, with τ_{rec} as a characteristic time for the temperature of the heated volume of the sample to decay back to the initial equilibrium temperature (5). The parameters that were varied when

matching the two traces were k_1, k_2, $I(0^+)$, I_1, $I(\infty)$ and the multiplicative scale factor needed to match the two traces. Once appropriately scaled, the two data sets were combined into a single kinetic trace that covered the time range from ~30 μs to 400 ms. The combined traces were then used for all subsequent analyses.

1.8 Measurements of T-jump size and recovery kinetics. The T-jump recovery kinetics traces were obtained from measurements on control (2AP-ref samples) that were shown to exhibit only the T-jump recovery kinetics. These measurements were carried out in a time-window of up to about 400 ms. The recovery kinetics were fitted to the following recovery function:

$$I(t) = [I(0^+) - I(0^-)]f_{rec}(t) + I(0^-) = [I(0^+) - I(0^-)]/(1 + t/\tau_{rec}) + I(0^-) \quad \text{(S13)}$$

with $I(0^+)$ and $I(0^-)$ as described above. The recovery time constant τ_{rec} was determined for each sample at room temperature and was found to be 108.5 ± 10.2 ms for VPK-2AP and 142.7 ± 8.4 ms for HP1-2AP.

The magnitude of the temperature jump was estimated by comparing the ratio of the fluorescence intensity levels $I(0^+)/I(0^-)$ of the reference sample (2AP-ref), measured in the T-jump spectrometer before and immediately after the T-jump, with the ratio of the fluorescence intensity levels $F(T_{fin})/F(T_{in})$, measured for 2AP-ref under equilibrium conditions at the initial (T_{in}) and final (T_{fin}) temperatures, such that $\frac{I(0^+)}{I(0^-)} = \frac{F(T_{fin})}{F(T_{in})}$. The value of T_{fin} that satisfied this condition was assigned as the final temperature in the T-jump measurements, corresponding to the temperature of the sample immediately after the IR pulse. The values of the size of the T-jump and the recovery time constant thus obtained were used as initial guesses in a global fit analysis, as described in the next section.

1.9 Global analysis of equilibrium and T-jump relaxation traces. To simultaneously describe the 2AP-probed equilibrium and kinetics measurements on hairpin HP1-2AP and pseudoknot VPK-2AP, we followed a global analysis approach described below.

The equilibrium melting profiles were parameterized in terms of a minimal kinetic scheme (two-state HP ⇔ U for HP1-2AP and three-state PK ⇔ pkHP1 ⇔ U for VPK-2AP at 50 mM KCl), as described in SI Methods 1.3. To describe the temporal change in the fluorescence signals in response to a T-jump perturbation, we used a master equation

approach to express the time-dependent change in the population of each macrostate in the kinetic scheme (6). The transitions between the various macrostates in the kinetic scheme were described in terms of a set of coupled differential equations:

$$\frac{dP_i}{dt} = \sum_{j \neq i} k_{j \to i} P_j - k_{i \to j} P_i \tag{S14}$$

where P_i (P_j) is the population of the *i*th (*j*th) macrostate and $k_{j \to i}$ and $k_{i \to j}$ are the rates for transitions from state j to state i and from state i to state j, respectively.

The matrix form of the master equation is:

$$\frac{d\mathbf{P}\,(t,T)}{dt} = \mathbf{M}(T) \cdot \mathbf{P}(t,T) \tag{S15}$$

where **P** is a column vector col($P_1, \ldots, P_\Omega$), and **M** is a $\Omega \times \Omega$ rate matrix with $M_{ij} = k_{j \to i}, i \neq j$ as the off-diagonal elements and $M_{ii} = -\sum_{j \neq 1} k_{i \to j}$ as the diagonal elements. The time-dependent solution of the rate equations yields the change in population as a function of time $\mathbf{P}(t,T)$, and is obtained by diagonalizing the matrix **M** to obtain its eigenvalues (λ_i) and eigenvectors (U_i).

The solution to Eq. S15 can be written as:

$$\mathbf{P}(t,T) = \exp[\mathbf{M}(T)t]\,\mathbf{P}(0) = \mathbf{U}\exp[\boldsymbol{\lambda}(T)t]\,\mathbf{U}^{-1}\mathbf{P}(0) \tag{S16}$$

where $\exp[\boldsymbol{\lambda}(T)t]$ is a $\Omega \times \Omega$ diagonal matrix with $\exp[\lambda_i(T)t]$ as the diagonal matrix elements, **U** is a $\Omega \times \Omega$ matrix consisting of the eigenvectors, and $\mathbf{P}(0)$ is the column vector representing the populations of all microstates at $t = 0$ (6). The eigenvalues and eigenvectors of the real non-symmetrical square matrices **M** were calculated using the built-in functions in MATLAB (R2014a 8.3.0.532) and the GNU Scientific Libraries (GSL 1.16) in C.

To model relaxation kinetics in response to a T-jump from an initial temperature T_{in} to a final temperature T_{fin}, the initial populations of the macrostates immediately after the T-jump were assumed to be identical to the equilibrium populations at T_{in}, i.e. $\mathbf{P}(t=0) = \mathbf{P_{eq}}(T_{in})$, and were calculated using Eq. S1. The final populations, after the relaxation is

complete, are expected to be consistent with the equilibrium populations at the final temperature, i.e. $\mathbf{P}(t=\infty, T_{fin}) = \mathbf{P_{eq}}(T_{fin})$.

The temperature dependence of the rate constants describing the transitions between the different macrostates were parameterized in terms of an Arrhenius equation:

$$k_{i\to j} = k^0_{i\to j}(T^0)\exp\left[-\frac{\Delta H^{\ddagger}_{i\to j}}{R}\left(\frac{1}{T}-\frac{1}{T^0}\right)\right] \tag{S17}$$

where $k^0_{i\to j}$ is the rate constant at a reference temperature T^0 and $\Delta H^{\ddagger}_{i\to j}$ is the enthalpy barrier for the transition from the *i*-th to the *j*-th macrostate. The backward rates $k_{j\to i}(T)$ were calculated from the forward rates as:

$$k_{j\to i}(T) = k_{i\to j}(T)\exp\left[-\frac{\Delta G_{jo}-\Delta G_{io}}{RT}\right] \tag{S18}$$

To model the relaxation kinetics, we first identified the intensity levels measured in the T-jump spectrometer prior to the arrival of the infrared heating pulse, $I(0^-)$, as characteristic of the fluorescence levels of the equilibrium population at the initial temperature. To match the fluorescence levels measured in the T-jump spectrometer with those measured in the equilibrium fluorescence measurements, we used a scale factor ς as follows:

$$I(0^-) = \varsigma F_{eq}(T_{in}) = \varsigma\sum_i F_i(T_{in})P_{i_{eq}}(T_{in}) \tag{S19}$$

The scale factor for each kinetics trace was then computed directly from the measured intensities in the two experimental setups: $\varsigma = I(0^-)/F_{eq}(T_{in})$. The time dependent change in fluorescence measured in the T-jump spectrometer in response to a T-jump, at $T_{fin} = T_{in} + \Delta T$, was written in terms of the time-dependent change in the population of the macrostates $P_i(t,T)$ from their initial population immediately after the T-jump, $\mathbf{P}(t=0) = \mathbf{P_{eq}}(T_{in})$, to the final population at the end of the relaxation kinetics, $\mathbf{P}(t=\infty, T_{fin}) = \mathbf{P_{eq}}(T_{fin})$, and the eventual recovery of this population back to $\mathbf{P_{eq}}(T_{in})$ as the T-jump itself recovers, as characterized by the $f_{rec}(t)$ function in Eq. S12:

$$I(t, T_{fin}) = \left[\varsigma\sum_i F_i(T_{fin})P_i(t, T_{fin}) - I(0^-)\right]f_{rec}(\mathrm{t}) + I(0^-) \tag{S20}$$

For a complete description of the equilibrium melting profiles and the relaxation kinetics traces in a self-consistent manner, the following variables were free parameters in our fitting algorithm: ΔH_{ji} and T_{mji} (to describe the free energy of each of the macrostates at all temperatures), $\Delta H^{\ddagger}_{i\to j}$ and $k^{0}_{i\to j}$ (to describe the forward rate constants between the macrostates at all temperatures, with the backward rates obtained from Eq. S18), F_{io} and m_i (to describe the fluorescence levels for each macrostate as a function of temperature), and ΔT and τ_{rec} for each kinetic trace. $I(0^{-})$ was obtained from each experimental trace, by averaging the fluorescence intensities measured in each trace prior to the T-jump perturbation, and T_{in} was obtained from measurements of the equilibrium sample temperature in the T-jump apparatus. The reference temperature for the relaxation rates was fixed at $T^{0} = 50$ °C for the pseudoknot to hairpin transition in VPK-2AP and at $T^{0} = 85$ °C for the hairpin to single-stranded RNA transition, for VPK-2AP and HP1-2AP.

The global analysis approach was first applied to measurements on HP1-2AP, using a two-state description to simultaneously fit the fluorescence melting profile and kinetics traces measured at 4 different temperatures (Figure 4). In the case of VPK-2AP, a three-state sequential scheme was used to simultaneously describe the fluorescence melting profile and kinetics traces measured at 9 different temperatures (Figure 5). The equilibrium populations of the three states at all temperatures were determined in terms of four parameters: the melting temperature and the enthalpy change for the PK⇔pkHP1 transition and the corresponding parameters for the pkHP1⇔U transition. The temperature dependencies of the fluorescence in each state were modeled as linear baselines, as explained in SI Methods 1.3. To characterize the kinetics traces, the time-dependent populations of the three states were obtained from a solution to a master equation, as described above, with the unfolding rate coefficients for each transition, $k_{PK\to pkHP1}$ and $k_{pkHP1\to U}$, determined in terms of two parameters each: the rate coefficients $k^{0}_{PK\to pkHP1}$ (at reference temperature of 50 °C) and $k^{0}_{pkHP1\to U}$ (at reference temperature of 85 °C), and their corresponding enthalpy barriers ($\Delta H^{\ddagger}_{PK\to pkHP1}$ and $\Delta H^{\ddagger}_{pkHP1\to U}$); the folding rates were determined from the unfolding rates and the equilibrium parameters as before. To constrain the parameter space, the equilibrium, kinetics and fluorescence baseline

parameters for the pkHP1⇔U transition in VPK-2AP were constrained to be close (though not identical) to the corresponding values obtained from the analysis of the HP1-2AP data.

The parameters that best described the HP1-2AP or VPK-2AP equilibrium and kinetics data were obtained using a simulated annealing fitting procedure (7–9). For HP1-2AP and VPK-2AP, 10,000 independent fitting procedures were performed. The fit parameters reported in the text and their uncertainties were determined by two different methods. In the first method, the fitting parameters and errors were calculated as the weighted ($w = 1/\chi_\nu^2$) average and standard deviation of the fitted parameters of all the fits between the range of 1-1.5 times the lowest χ_ν^2 obtained in independent fitting procedures. Here, χ_ν^2 is the reduced chisq, defined as χ^2 (Eq. S11) divided by the number of data points minus the number of parameters. In the second method, the uncertainties in the parameters were determined by the procedure described in SI Methods 1.5; these uncertainties are reported inside parentheses in SI Table S3. The values of the final temperatures reported in the kinetic traces shown in Figures 4 and 5 were obtained from the average T-jump obtained from the global fit for that set, for example from the average of the parameter ΔT for each of the 4 kinetics traces in Figure 4 and 9 kinetics traces in Figure 5.

The melting and kinetics fitting parameters allow the determination of the folding/unfolding rates at different temperatures, as specified in Eqs. S17 and S18. For unfolding, the uncertainties in these rates as a function of temperature were estimated in the following way:

$$\sigma^-_{k_{i\to j}}\left(\sigma_{k^0_{i\to j}}\right) = \left[k^0_{i\to j}(T^0) - \sigma_{k^0_{i\to j}}\right]\exp\left[-\frac{\Delta H^\ddagger_{i\to j}}{R}\left(\frac{1}{T}-\frac{1}{T^0}\right)\right] \tag{S21}$$

$$\sigma^+_{k_{i\to j}}\left(\sigma_{k^0_{i\to j}}\right) = \left[k^0_{i\to j}(T^0) + \sigma_{k^0_{i\to j}}\right]\exp\left[-\frac{\Delta H^\ddagger_{i\to j}}{R}\left(\frac{1}{T}-\frac{1}{T^0}\right)\right] \tag{S22}$$

$$\sigma^-_{k_{i\to j}}\left(\sigma_{\Delta H^\ddagger_{i\to j}}\right) = k^0_{i\to j}(T^0)\exp\left[-\frac{\left(\Delta H^\ddagger_{i\to j} - \sigma_{\Delta H^\ddagger_{i\to j}}\right)}{R}\left(\frac{1}{T}-\frac{1}{T^0}\right)\right] \tag{S23}$$

$$\sigma^+_{k_{i\to j}}\left(\sigma_{\Delta H^\ddagger_{i\to j}}\right) = k^0_{i\to j}(T^0)\exp\left[-\frac{\left(\Delta H^\ddagger_{i\to j} + \sigma_{\Delta H^\ddagger_{i\to j}}\right)}{R}\left(\frac{1}{T}-\frac{1}{T^0}\right)\right] \tag{S24}$$

The rates obtained using the uncertainties from each of these equations S21-S24 are contained within a range defined by a lower (–) or upper limit (+), as determined by the errors of the fitting parameters $k_{i\to j}^{0}(T^{0})$ and $\Delta H_{i\to j}^{\ddagger}$; this range was thus taken as a measure of the uncertainty in the determination of the rates (see SI Figure S6). The uncertainties in the folding rate coefficients $k_{j\to i}(T)$ were calculated in a similar manner and were dependent on the uncertainties of the unfolding rate coefficients $k_{i\to j}(T)$ (Eqs. S21-S24), and in the uncertainties of ΔG_{ji}, which in turn were determined by the uncertainties in the fitting parameters ΔH_{ji} and T_{mij}, Eq. S3. The unfolding/folding rate coefficients $k_{i\to j/j\to i}(T)$, computed at 37 °C are reported in SI Table S3.

1.10 Simulation details. We performed molecular dynamics simulations using a coarse-grained RNA model. The model and parameters were calibrated and described in detail elsewhere (10). In the model, each nucleotide is represented by three interaction sites (TIS) corresponding to a phosphate, ribose sugar, and base. Briefly, the effective potential energy of a given RNA conformation is $U = U_L + U_{EV} + U_{ST} + U_{HB} + U_{EL}$, where U_L accounts for chain connectivity and angular rotation of the polynucleic acids, U_{EV} accounts for excluded volume interactions, U_{ST} and U_{HB} are the base-stacking and hydrogen-bond interactions, respectively. The last term U_{EL} is electrostatic interactions between phosphate groups, depending on a given salt concentration. Electrostatic interactions are taken into account using the Debye-Hückel theory to reproduce salt-dependent thermodynamics of RNA. The charges on the phosphates were determined using the counter ion condensation theory. The parameters in the TIS model were calibrated with thermodynamics of dinucleotides, several hairpins, and pseudoknots so that experimental data such as heat capacities are reproduced (10). The same model was also used to study another pseudoknot, BWYV PK, and verified to reproduce experimentally-obtained thermodynamics data (11). In particular for this study, we confirmed that the model gives excellent consistency with experimental heat capacity at both 50 mM and 1M monovalent salt (SI Figure S15). To obtain an equilibrium ensemble at 50 mM and 1 M, we used the temperature replica-exchange technique with low-friction Langevin dynamics to enhance the sampling efficiency (12, 13). For kinetic simulations, we first prepared the unfolded conformations by running simulations at 120 °C. Starting from the unfolded conformations, Brownian

dynamics simulations under realistic water viscosity ($\eta = 10^{-3}$ Pa·s) were performed until each trajectory folded to the PK state at 37 °C. The same procedure was repeated at different salt concentrations of 50, 100, 200, 500, 800 mM and 1M. For each condition, we generated more than 200 folding trajectories. Each trajectory is categorized either pkHP1 or pkHP2 pathway according to which stem is folded earlier than the other. Each stem is deemed "folded" if all the base pairs are formed ($U_{HB} < k_BT$). For the purpose of converting simulation time into real time, we consider the characteristic time of the Brownian dynamics, $\tau = \frac{6\pi\eta a^3}{k_B T} \approx 300$ ps, where we use $a = 4$ Å as the typical length scale; because we integrate the motion by a small fraction of time, a single simulation step corresponds to 3 ps (14, 15).

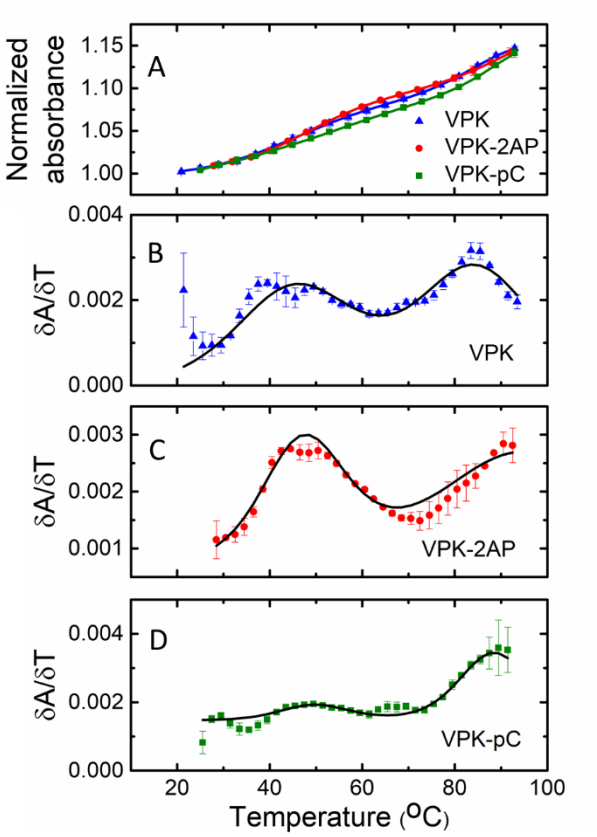

Figure S1. Thermodynamics of VPK melting from absorbance experiments at 50 mM KCl. (*A*) The absorbance values of VPK, VPK-2AP and VPK-pC, measured at 260 nm, are plotted as a function of temperature. The absorbance profiles are normalized by dividing each curve by the absorbance measured at the lowest temperature, at 20 °C. The data (symbols) are the averages of 2–3 independent sets of measurements: three experiments were done for VPK: one at 10 μM strand concentration and two at 18.5 μM; two experiments were done for VPK-pC at 1.7 μM and two for VPK-2AP at 12.6 μM concentration. (*B–D*) The first derivative of the absorbance with respect to temperature ($\delta A/\delta T$) is plotted as a function of temperature for (*B*) VPK, (*C*) VPK-2AP and (*D*) VPK-pC. The continuous lines in all the panels are fits to a three-state sequential model PK ⇔ pkHP ⇔ U, with fitting parameters summarized in SI Table S1. Unlabeled VPK exhibits two melting transitions: PK ⇔ pkHP at ~47 °C and pkHP ⇔ U at ~85 °C; the corresponding transitions for VKP-2AP occur at ~48 °C and ~97 °C, and for VPK-pC at ~53 °C and ~89 °C. For all panels, the error bars represent the standard error of the mean (SEM); error bars not visible are smaller than the symbols. For clarity, only every other data point is presented.

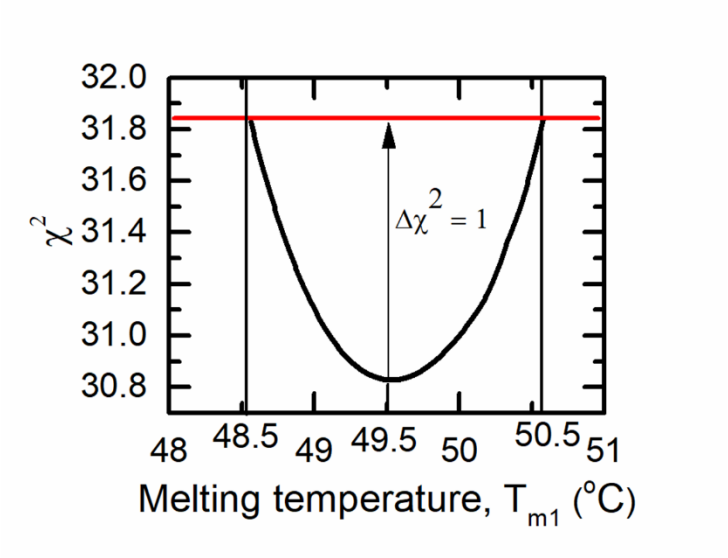

Figure S2. Estimation of uncertainty in fitting parameters. The plot illustrates how the variation in χ^2 as a function of a parameter in a fit is used to estimate the uncertainty in that parameter. The χ^2 values obtained from a fit to the VPK-2AP fluorescence melting profile, for the data shown in Figure 5b, are plotted as a function of the melting temperature for the PK ⇔ pkHP transition; χ^2 values were found as described in SI Methods 1.5. The horizontal red line indicates the $\Delta\chi^2 = 1$ level, which was used as a cutoff for the uncertainties in that parameter, as indicated by the vertical lines. In this example, the value of the parameter and its uncertainty thus estimated is reported as $49.5^{+1.0}_{-1.0}$ °C.

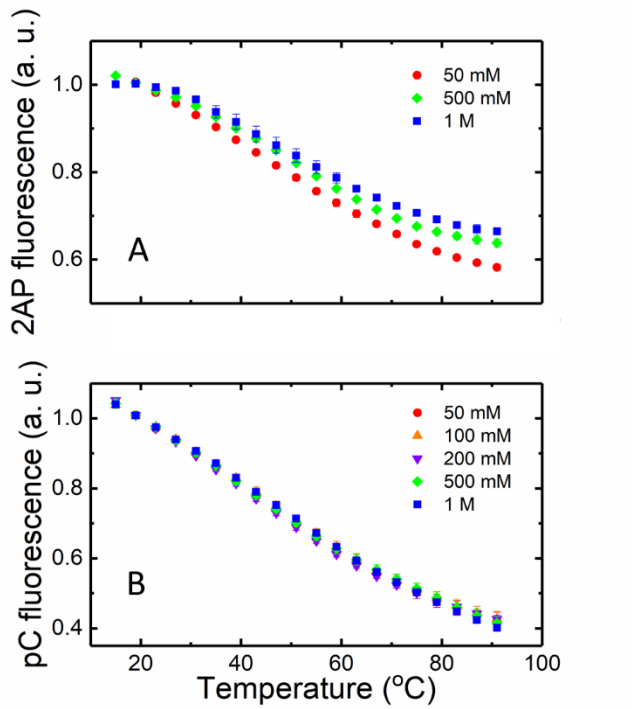

Figure S3. Equilibrium fluorescence measurements on 2AP and pC control samples. The fluorescence intensities as a function of temperature are plotted for (*A*) 2AP-ref (5'-CC[2AP]CU-3'), with excitation at 310 nm, and for (*B*) pC-ref (5'-GC[pC]CA-3'), with excitation at 350 nm. All measurements were done in 10 mM MOPS buffer pH 7.0, but at different monovalent salt conditions, as indicated in each of the panels. The data (symbols) are the average of two independent sets of measurements, and were normalized to match at 20 °C. The error bars represent the SEM; error bars not visible are smaller than the symbols. For clarity, only every other data point is presented.

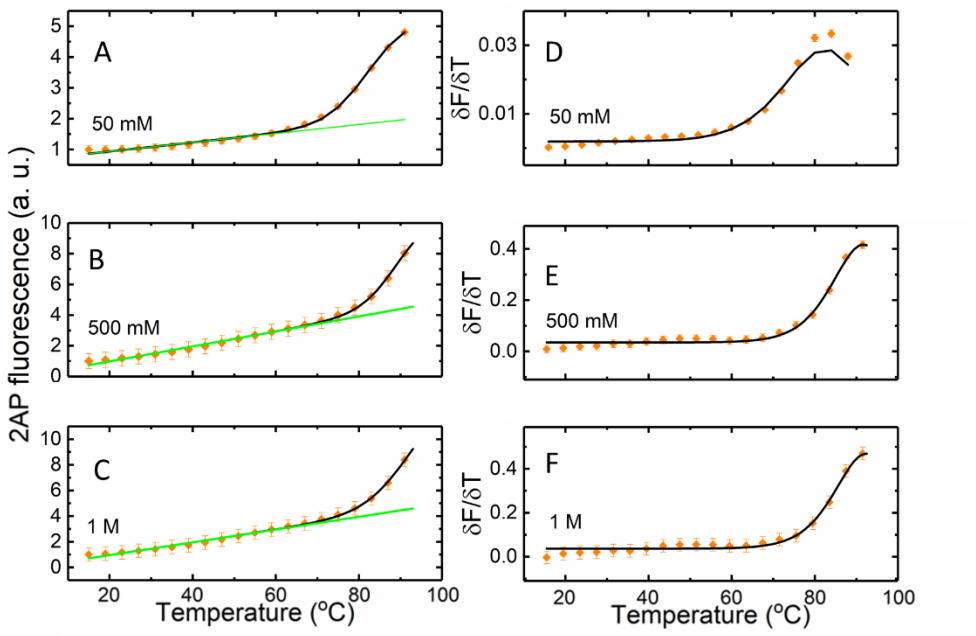

Figure S4. Thermodynamics of HP1-2AP melting from fluorescence measurements. The fluorescence intensities of the 2AP probe (left) and the corresponding first derivatives $\delta F/\delta T$ (right) are plotted as a function of temperature for HP1-2AP in (*A*,*D*) 50 mM KCl; (*B*,*E*) 500 mM NaCl; and (*C*,*F*) 1 M NaCl. The error bars represent the SEM; error bars not visible are smaller than the symbols. For clarity, only every other data point is presented. The continuous black lines are fits to a two-state transition, with T_m ~84 °C, ~91 °C, and ~94 °C, at 50 mM, 500 mM and 1 M monovalent salt concentrations; the green lines in each panel correspond to the baselines for the folded hairpin state as obtained from the fits; the baselines for the unfolded state were constrained to have the same slope as that for the corresponding measurements on the reference 2AP-ref samples (from SI Figure S3*A*). The thermodynamic parameters obtained from the fits are summarized in SI Table S2.

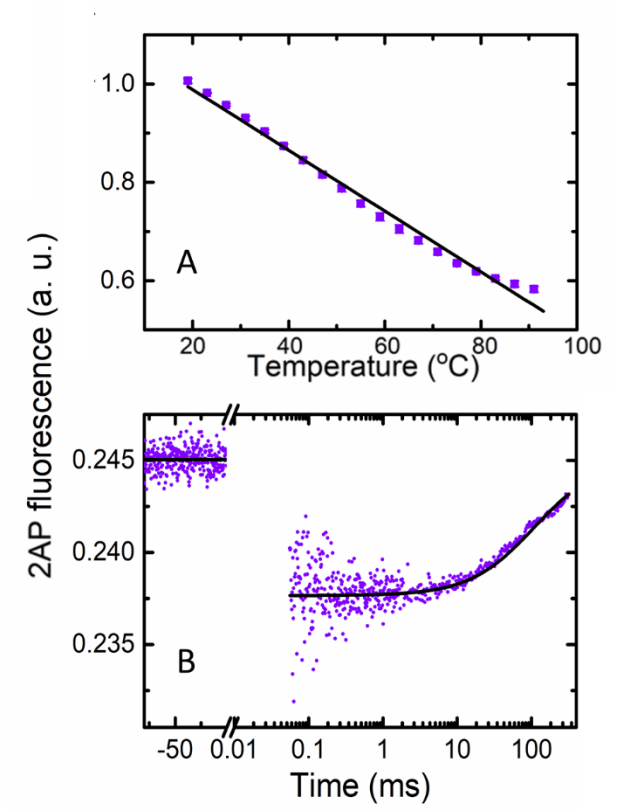

Figure S5. Equilibrium fluorescence and T-jump measurements on the control sample 2AP-ref at 50 mM KCl. (*A*) The fluorescence of 2AP-ref, with excitation at 310 nm, is plotted as a function of temperature. The data are identical to those shown in SI Figure S3*A*. The error bars represent the SEM from two independent sets of measurements; error bars not visible are smaller than the symbols. For clarity, only every other data point is presented. The continuous black line is a linear fit to the data. (*B*) The fluorescence intensities measured on a 2AP-ref sample in the T-jump spectrometer are plotted as a function of time. The negative values for time on the x-axis indicate measurements prior to the arrival of the IR pulse that induces the T-jump in the sample. Immediately after the T-jump, the fluorescence in the sample drops, as a result of the change in the quantum yield of 2AP. The fluorescence then decays back to the pre-T-jump levels. The continuous line is a fit to the data, using the T-jump recovery function described by Eq. S12, with a characteristic recovery time constant $\tau_{rec} = 143$ ms.

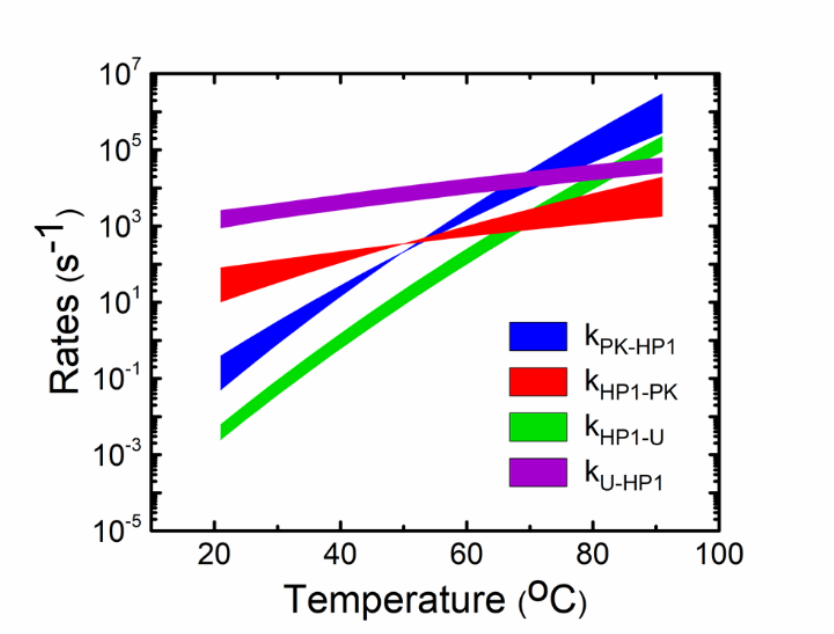

Figure S6. Folding/unfolding rates of VPK-2AP. The rate constants for transitions between the three states depicted in Figure 5a, calculated using the parameters obtained from the global fit to the data in Figure 5, are plotted as a function of temperature. The widths of the lines represent the range of rate constants that are within one standard deviation of the best fit parameters, and include uncertainties from both the rate constants at a reference temperature T^0 (Eq. S17) as well as the uncertainties in the activation enthalpy parameters; this range was computed as described in SI Methods 1.9 (Eqs. S21-S24).

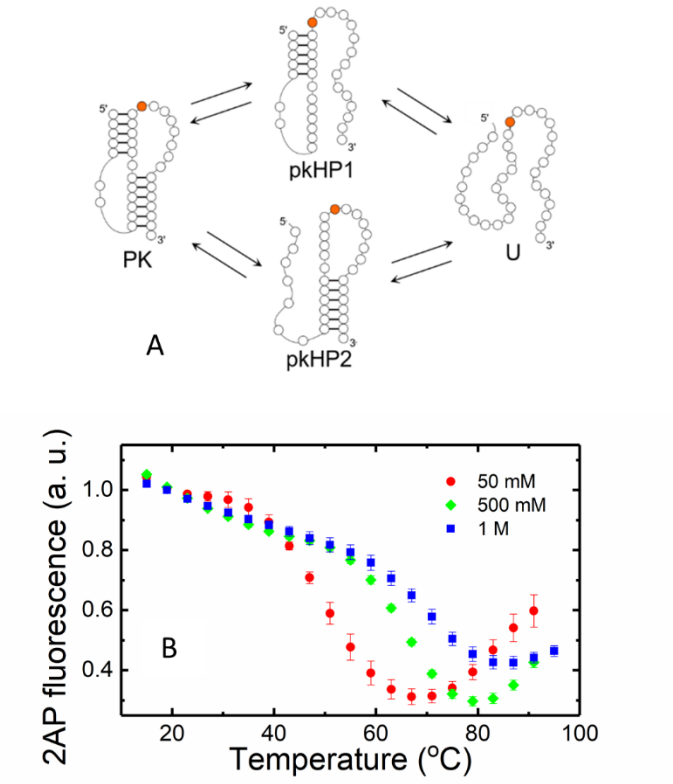

Figure S7. Thermodynamics of VPK-2AP melting from fluorescence measurements at different salt conditions. (*A*) Four-state parallel pathway scheme is shown for VPK with the 2AP probe in each of the folded/unfolded conformations shown in red. (*B*) 2AP fluorescence intensities as a function of temperature are plotted for VPK-2AP, with excitation at 310 nm, at three different monovalent salt conditions: 50 mM KCl (red); 500 mM NaCl (green); and 1 M NaCl (blue). The data (symbols) are the averages of 2–3 independent sets of measurements. The error bars represent the SEM; error bars not visible are smaller than the symbols. For clarity, only every other data point is presented.

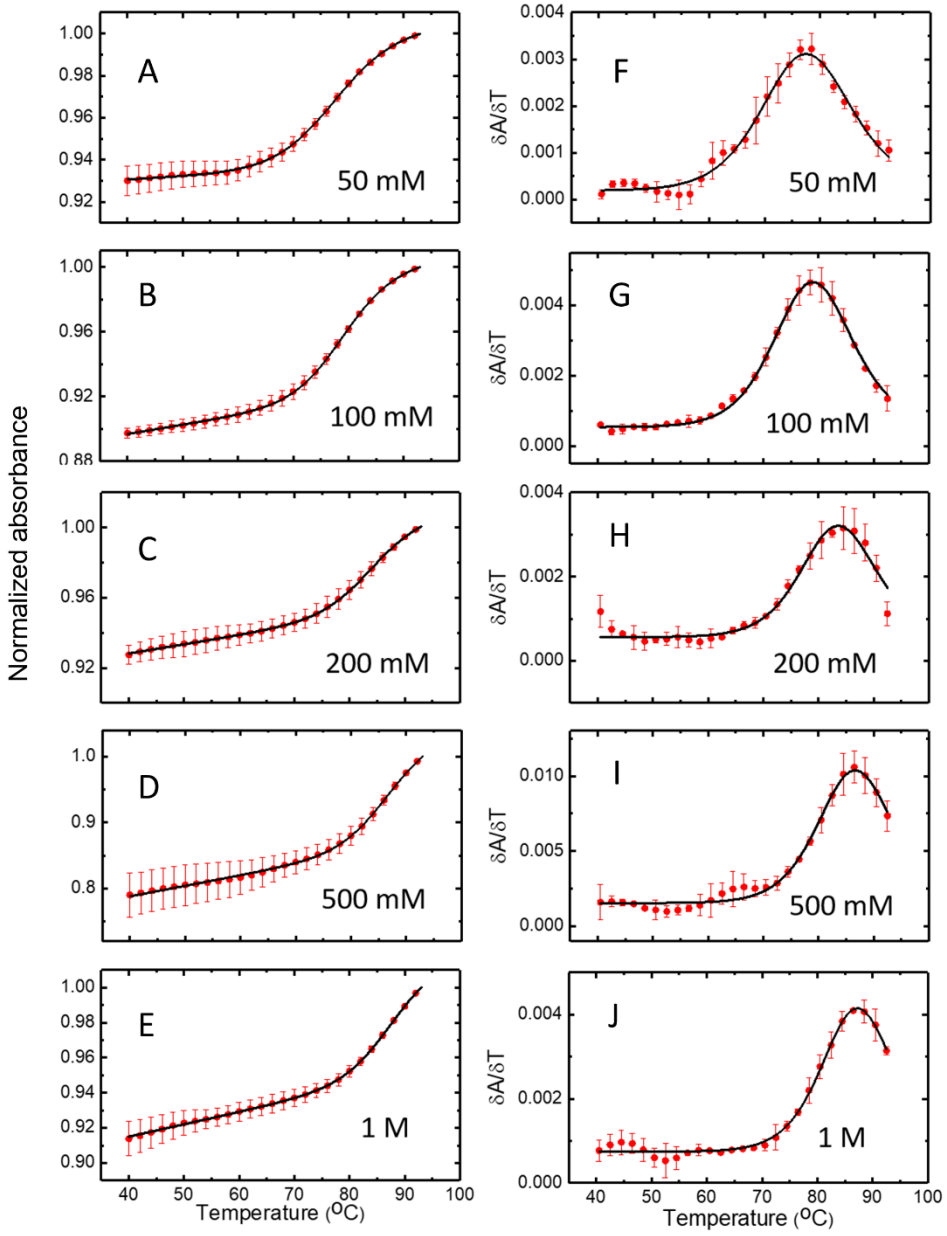

Figure S8. Thermodynamics of unlabeled HP1 melting from absorbance experiments. (*A-E*) The absorbance values of unlabeled HP1, measured at 260 nm, are plotted as a function of temperature, for measurements at different monovalent salt conditions. The absorbance profiles were normalized by dividing each curve by the absorbance measured at the highest temperature, at 91 °C. (*F-J*) The corresponding first derivatives of the absorbance with respect to temperature ($\delta A/\delta T$) are plotted as a function of temperature. The error bars represent the SEM; error bars not visible are smaller than the symbols. For clarity, only every other data point is presented. The continuous lines are fits to a two-state model; the fitting parameters are summarized in SI Table S2.

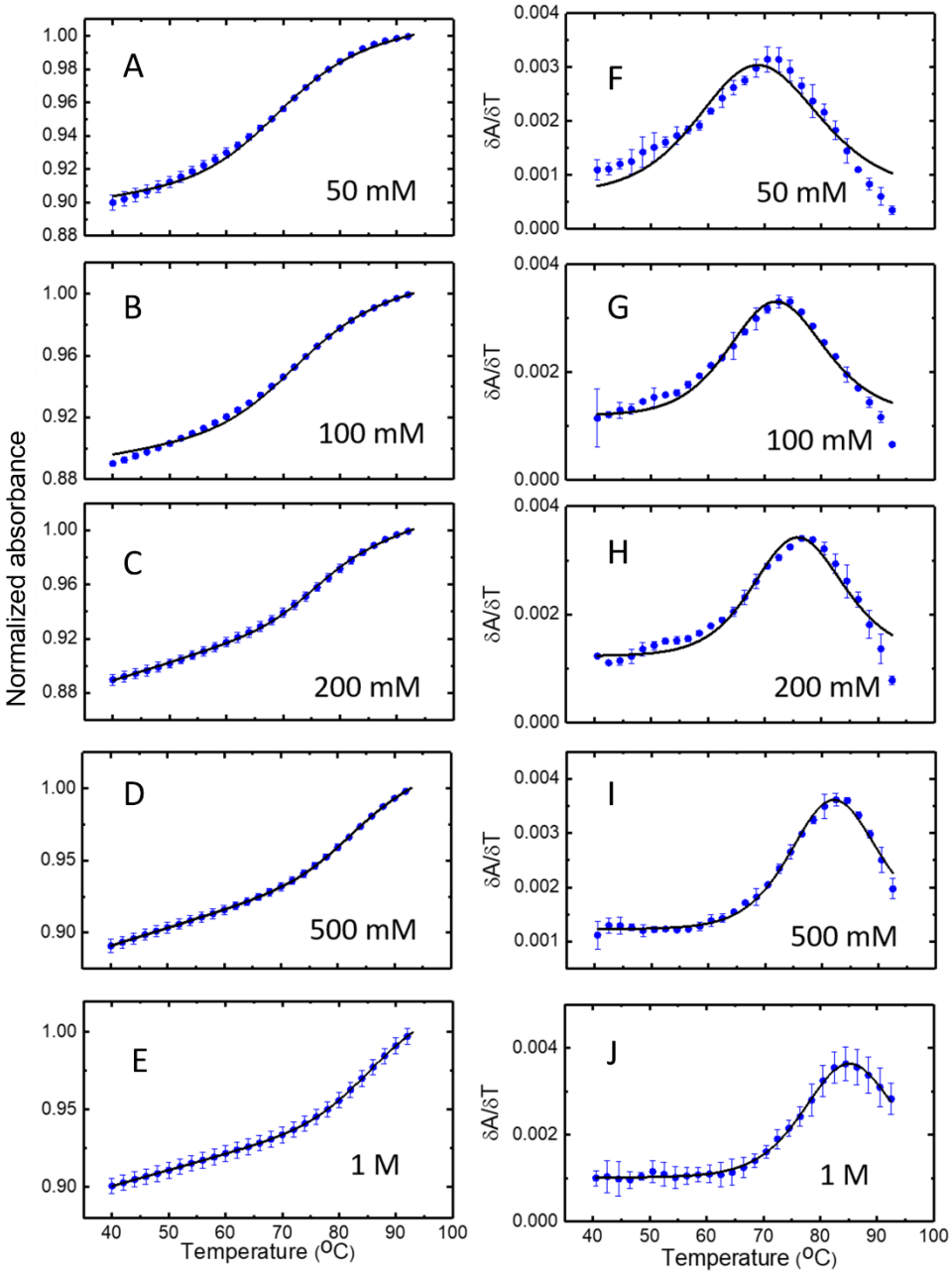

Figure S9. Thermodynamics of unlabeled HP2 melting from absorbance experiments. The panels are as described for SI Figure S8. The error bars represent the SEM; error bars not visible are smaller than the symbols. For clarity, only every other data point is presented. The continuous lines are fits to a two-state model; the fitting parameters are summarized in SI Table S4.

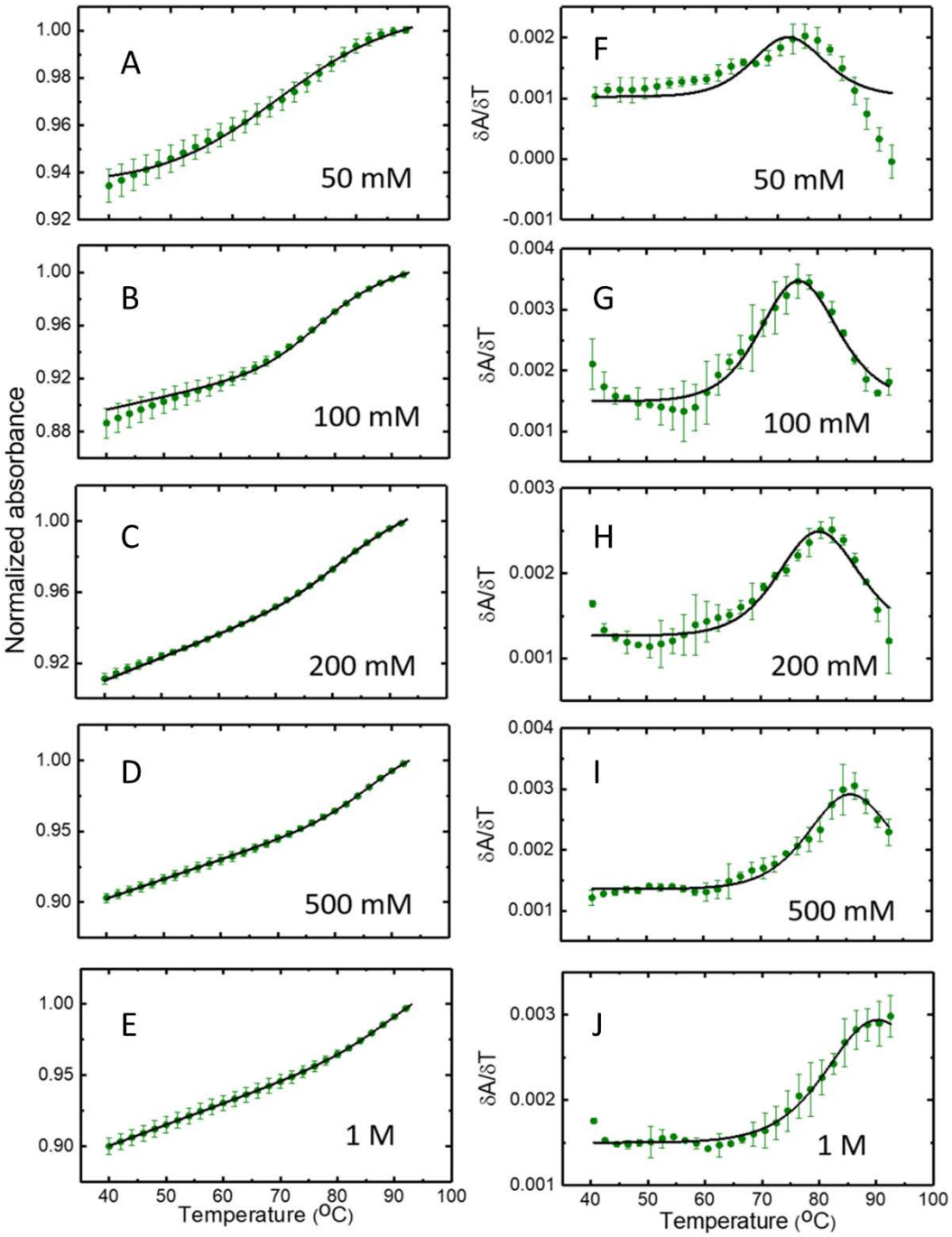

Figure S10. Thermodynamics of labeled HP2-pC melting from absorbance experiments. The panels are as described for SI Figure S8. The error bars represent the SEM; error bars not visible are smaller than the symbols. For clarity, only every other data point is presented. The continuous lines are fits to a two-state model; the fitting parameters are summarized in SI Table S4.

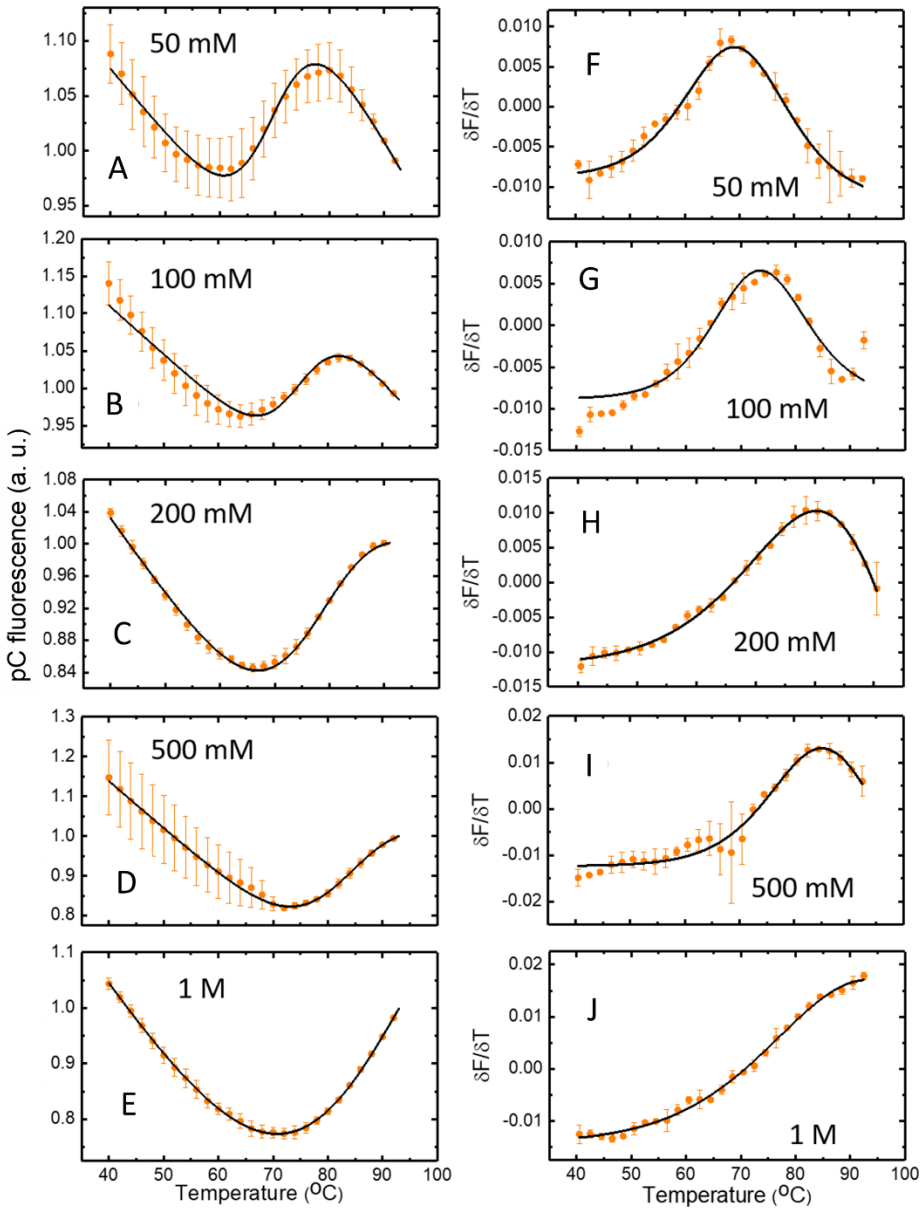

Figure S11. Thermodynamics of labeled HP2-pC melting from fluorescence measurements. The fluorescence intensities of the pC probe (*A*-*E*) and the corresponding first derivatives $\delta F/\delta T$ (*F*-*J*) are plotted as a function of temperature for HP2-pC, for measurements at different monovalent salt concentrations. The error bars represent the SEM; error bars not visible are smaller than the symbols. For clarity, only every other data point is presented. The continuous black lines are fits to a two-state transition, with the baselines for the unfolded state constrained to have the same slope as that for the corresponding measurements on the reference pC-ref samples (from SI Figure S3*B*). The thermodynamic parameters obtained from the fits are summarized in SI Table S4.

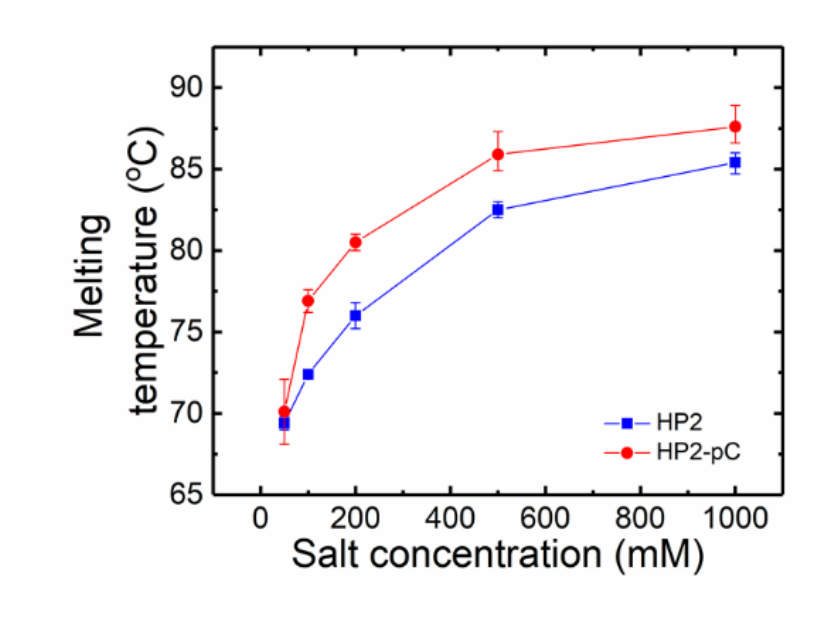

Figure S12. Effect of pC probe on the stability of hairpin HP2. The melting temperatures of unlabeled HP2 (blue squares) and pC-labeled HP2-pC (red circles) are plotted as a function of the monovalent salt concentrations. The data (symbols) are the average of the parameters obtained from fits to the absorbance melting profiles and to the corresponding derivatives. For each set of fits, the errors in the parameters were obtained as described in SI Methods 1.5. The error bars in the figure represent the compounded errors calculated from the fits to melting profiles (σ_m) and fits to derivatives (σ_d) as: $\sigma = \frac{\sqrt{\sigma_m^2+\sigma_d^2}}{2}$; error bars not visible are smaller than the symbols.

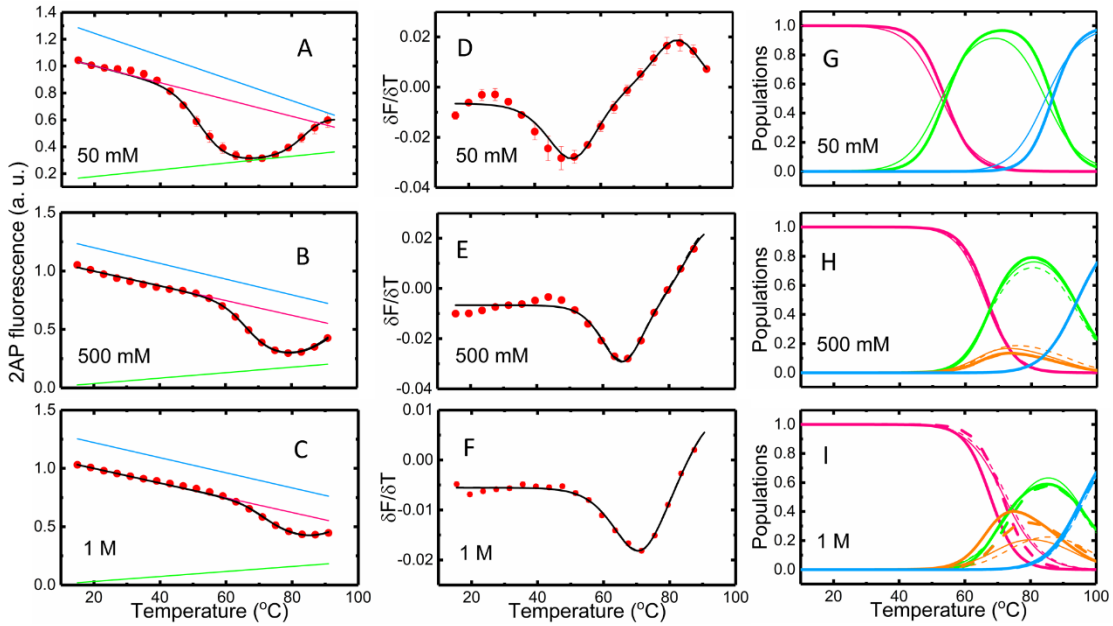

Figure S13. Four-state parallel pathway description of the VPK-2AP fluorescence melting profiles. (*A*-*C*) The fluorescence melting profile of VPK-2AP, measured at 50 mM KCl (top), 500 mM NaCl (middle), and 1 M NaCl (bottom) are fitted to a 4-state parallel pathway model, as described in SI Methods 1.4. The baselines shown are for the fully folded PK state (pink) and for the partially folded hairpin pkHP1 (green); the baseline for the fully unfolded state U (blue) is constrained to have the same slope as that of the 2AP-ref sample; the baseline for pkHP2 (blue) is assumed identical to that of PK. (*D*-*F*) Corresponding fits to the 4-state model are shown for the derivative data $\delta F/\delta T$ versus temperature. The error bars in panels (*A*-*F*) represent the SEM; error bars not visible are smaller than the symbols. For clarity, only every other data point is presented. (*G*-*I*) The populations of the four states, obtained from the fits, are plotted as a function of temperature: PK (pink); pkHP1 and pkHP2 (green and orange, respectively); and U (blue). Four sets of populations are shown: two from fits to the VPK-2AP melting profiles (thick lines) and two from fits to the derivatives (thin lines), with either the PK ⟺ pkHP1 or the PK ⟺ pkHP2 transition temperature constrained from the simulation results (continuous and dashed lines, respectively). The thermodynamic parameters obtained from these fits are summarized in SI Table S5.

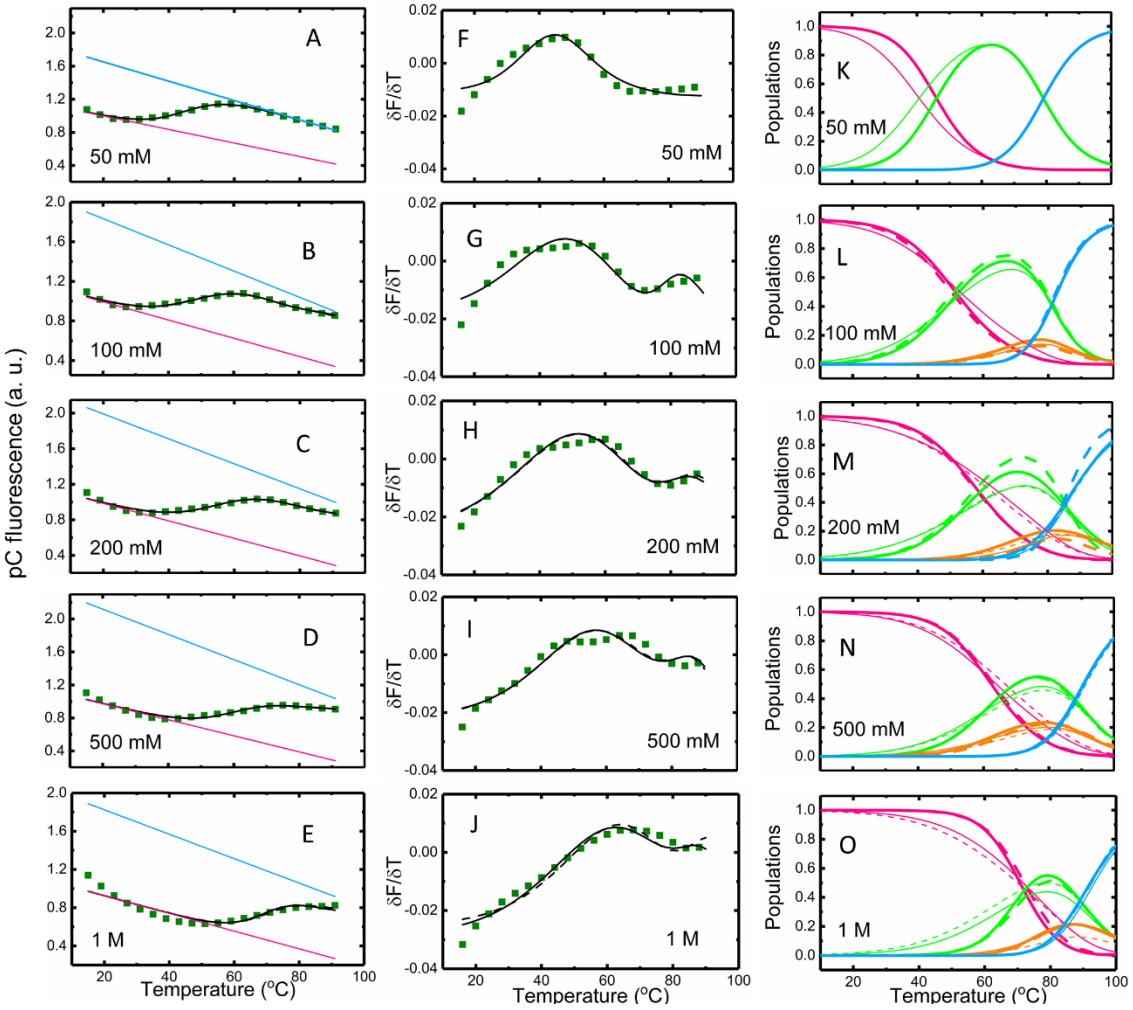

Figure S14. Four-state parallel pathway description of VPK-pC fluorescence melting profiles. (*A*-*E*) The fluorescence melting profile of VPK-pC, measured at (*A*) 50 mM KCl, (*B*) 100 mM NaCl, (*C*) 200 mM NaCl, (*D*) 500 mM NaCl and (*E*) 1 M NaCl are fitted to a 4-state model, as described in SI Methods 1.4. The baselines shown are for the fully folded PK state (pink) and the fully unfolded state (blue); baselines for pkHP1 are assumed identical to that for U, while the baselines for pkHP2 are assumed identical to that of PK. (*F*-*J*) Corresponding fits are shown for the derivative data $\delta F/\delta T$ versus temperature. The error bars in panels (*A*-*J*) represent the SEM; error bars not visible are smaller than the symbols. For clarity, only every other data point is presented. (*K*-*O*) The populations of the four states, obtained from the fits, are plotted as a function of temperature: PK (pink); pkHP1 and pkHP2 (green and orange, respectively); and U (blue). Four sets of populations are shown: two from fits to the VPK-2AP melting profiles (thick lines) and two from fits to the derivatives (thin lines), with either the PK ⇔ pkHP1 or the PK ⇔ pkHP2 transition temperature constrained from the simulation results (continuous and dashed lines, respectively). The thermodynamic parameters from these fits are in SI Table S6.

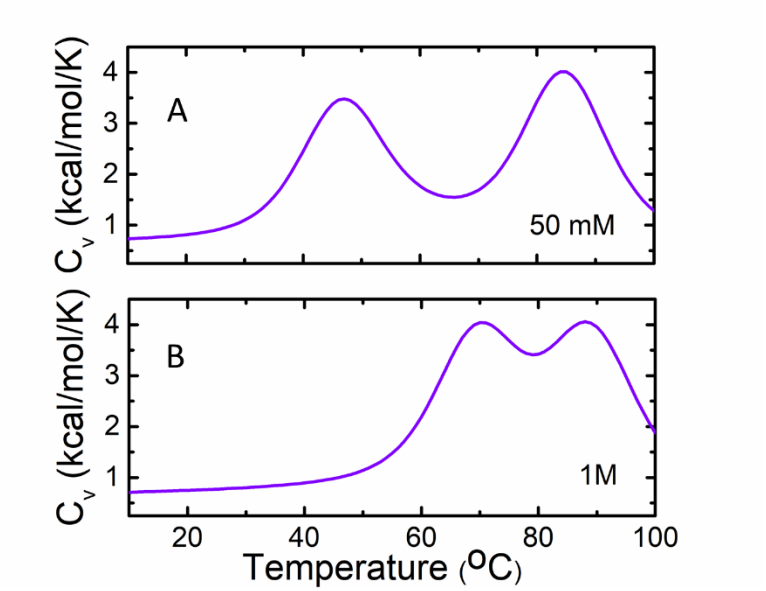

Figure S15. Thermodynamics of VPK obtained by equilibrium simulations at 50 mM and 1 M salt concentrations. (*A*) Heat capacity of VPK at 50 mM. The two observed transitions are at 47°C and 84°C. (*B*) Same as (*A*) but at 1M salt concentration. The two transitions in (*B*) occur at 70°C and 88°C.

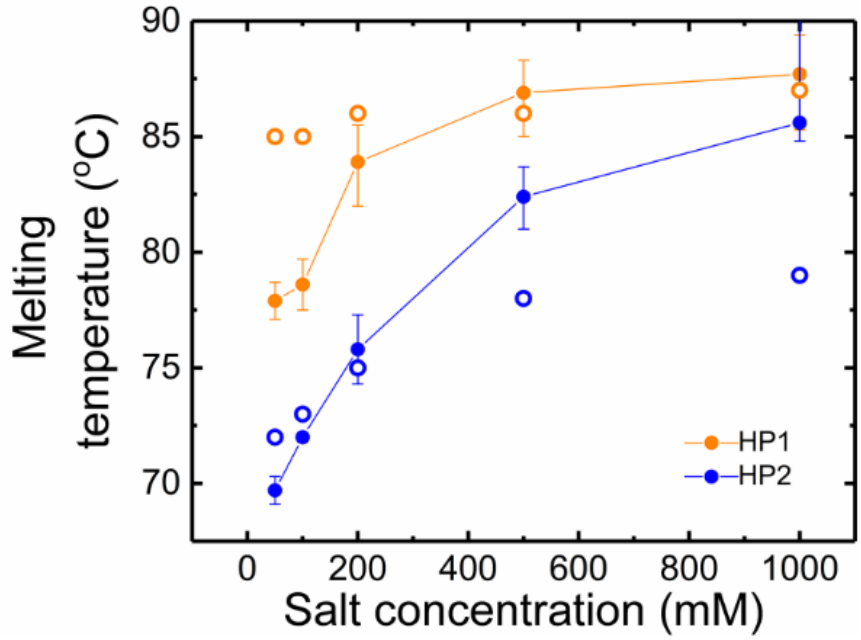

Figure S16. Salt dependence of the stability of hairpins HP1 and HP2. The melting temperatures of unlabeled HP1 (orange) and HP2 (blue) are plotted as a function of the monovalent salt concentrations. The data (filled symbols) are the average of the parameters obtained from fits to the absorbance melting profiles and to the corresponding derivatives. For each set of fits, the errors in the parameters were obtained as described in SI Methods 1.5. The error bars in the figure represent the compounded errors calculated from the fits to melting profiles (σ_m) and fits to derivatives (σ_d) as: $\sigma = \frac{\sqrt{\sigma_m^2+\sigma_d^2}}{2}$; error bars not visible are smaller than the symbols. The melting temperatures obtained from simulations on the isolated hairpins are also shown (open symbols).

Table S1. Thermodynamic parameters of unlabeled and labeled VPK at 50 mM KCl[a]

		Absorbance			Fluorescence	
		VPK	**VPK-2AP**	**VPK-pC**	**VPK-2AP**	**VPK-pC**
PK ⇔ pkHP1[b]	T_m **(°C)**	$47.2^{+2.6}_{-2.6}$ $(46.6^{+0.4}_{-0.4})$	$48.6^{+1.1}_{-1.0}$ $(47.5^{+0.1}_{-0.1})$	$56.1^{+4.3}_{-2.1}$ $(50.1^{+0.3}_{-0.3})$	$49.5^{+1.0}_{-1.0}$ $(50.8^{+1.4}_{-0.6})$	$46.0^{+0.5}_{-0.5}$ $(46.1^{+1.1}_{-0.5})$
	ΔH **(kcal/mol)**	$18.8^{+12.6}_{-2.9}$ $(23.0^{+0.7}_{-0.7})$	$24.7^{+12.1}_{-1.7}$ $(31.6^{+0.8}_{-0.8})$	$14.5^{+13.8}_{-9.6}$ $(23.8^{+2.7}_{-2.6})$	$58.2^{+10.5}_{-8.7}$ $(43.1^{+3.2}_{-3.2})$	$31.2^{+1.7}_{-1.6}$ $(27.0^{+0.7}_{-0.6})$
pkHP1 ⇔ U[c]	T_m **(°C)**	$85.3^{+1.6}_{-1.6}$ $(85.5^{+0.3}_{-0.3})$	$96.7^{+10.0}_{-7.6}$ $(97.0^{+0.9}_{-0.3})$	$88.5^{+2.8}_{-1.7}$ $(88.8^{+0.3}_{-0.2})$	$84.9^{+2.0}_{-2.2}$ $(87.0^{+1.6}_{-0.4})$	$79.0^{+0.2}_{-0.2}$ $(78.8^{+0.6}_{-0.4})$
	ΔH **(kcal/mol)**	$38.8^{+11.9}_{-10.2}$ $(30.9^{+1.4}_{-1.4})$	$26.3^{+19.7}_{-2.9}$ $(20.5^{+0.5}_{-0.5})$	$54.3^{+10.0}_{-9.2}$ $(46.0^{+2.2}_{-2.1})$	$49.4^{+10.7}_{-6.0}$ $(35.0^{+3.1}_{-2.3})$	$40.0^{+8.0}_{-5.4}$ $(40.0^{+2.5}_{-2.0})$

[a] Thermodynamic parameters are from fits to the absorbance or fluorescence melting profiles using a 3-state model, as described in SI Methods 1.3; parameters in parenthesis are from fits to the corresponding derivatives. The errors in the parameters were calculated as described in SI Methods 1.5. The melting temperatures reported in the text are the average of the values from the two different fits, rounded to the nearest integer. [b,c] PK: pseudoknot; pkHP1: hairpin 1 in the pseudoknot context; U: fully unfolded state.

Table S2. Thermodynamic parameters of unlabeled HP1 and labeled HP1-2AP at different salt concentrations[a]

	HP1 absorbance		**HP1-2AP fluorescence**	
Salt concentration (mM)	**ΔH (kcal/mol)**	**T_m (°C)**	**ΔH (kcal/mol)**	**T_m (°C)**
50	$44.2^{+6.6}_{-5.9}$ ($44.5^{+2.0}_{-1.9}$)	$77.8^{+0.4}_{-0.4}$ ($77.9^{+0.2}_{-0.2}$)	$49.6^{+2.5}_{-2.5}$ ($35.7^{+0.4}_{-0.4}$)	$82.9^{+0.2}_{-0.2}$ ($85.4^{+0.2}_{-0.2}$)
100	$54.7^{+4.0}_{-3.8}$ ($51.6^{+1.2}_{-1.2}$)	$79.1^{+0.2}_{-0.2}$ ($79.1^{+0.1}_{-0.1}$)	------	------
200	$55.0^{+12.9}_{-11.2}$ ($55.2^{+2.8}_{-2.7}$)	$84.1^{+0.8}_{-0.7}$ ($83.8^{+0.3}_{-0.3}$)	------	------
500	$58.0^{+14.2}_{-12.6}$ ($56.1^{+3.4}_{-3.3}$)	$86.8^{+0.9}_{-0.6}$ ($86.9^{+0.3}_{-0.3}$)	$58.6^{+5.5}_{-5.4}$ ($50.5^{+4.3}_{-1.0}$)	$90.9^{+1.3}_{-1.3}$ ($93.5^{+2.1}_{-1.5}$)
1000	$58.2^{+10.3}_{-9.5}$ ($58.9^{+2.8}_{-2.7}$)	$87.7^{+1.0}_{-0.7}$ ($87.5^{+0.3}_{-0.3}$)	$49.8^{+8.1}_{-5.2}$ ($50.6^{+5.4}_{-4.1}$)	$93.9^{+1.5}_{-1.0}$ ($94.4^{+3.3}_{-1.2}$)

[a]Thermodynamic parameters are from fits to the absorbance or fluorescence melting profiles using a 2-state model, as described in SI Methods 1.3; parameters in parenthesis are from fits to the corresponding derivatives. The errors in the parameters were calculated as described in SI Methods 1.5. The melting temperatures reported in the text are the average of the values from the two different fits, rounded to the nearest integer.

Table S3. Folding/unfolding parameters for VPK-2AP and HP1-2AP obtained from global modeling of thermodynamics and kinetics [a]

Transition	PK ⇔ pkHP1[b]	pkHP1 ⇔ U[b]	HP1 ⇔ U[c]
ΔH_{ji} (kcal/mol)	31.4 ± 5.0 $(28.7^{+0.3}_{-0.3})$	42.9 ± 1.8 $(42.0^{+1.8}_{-1.8})$	40.6 ± 3.2 $(41.4^{+0.6}_{-0.6})$
T_{mji} (°C)	53.2 ± 1.5 $(54.4^{+0.1}_{-0.1})$	83.2 ± 2.3 $(81.9^{+0.1}_{-0.1})$	87.3± 1.9 $(86.9^{+0.1}_{-0.1})$
$\Delta H^{\ddagger}_{i\to j}$ (kcal/mol)	47.6 ± 6.7 $(44.8^{+3.8}_{-4.0})$	57.7 ± 1.7 $(53.5^{+21.0}_{-ND})$	47.6 ± 4.6 $(48.6^{+5.1}_{-6.5})$
$k^{0}_{i\to j}$ (at T^0) (s^{-1})	$10^{2.3 \pm 0.1}$ $(10^{\,2.3^{+0.1}_{-0.1}})$ (T^0 = 50 °C)	$10^{4.6 \pm 0.2}$ $(10^{4.8^{+ND}_{-0.3}})$ (T^0 = 85 °C)	$10^{4.5 \pm 0.1}$ $(10^{4.5^{+0.2}_{-0.2}})$ (T^0 = 85 °C)
$\Delta H^{\ddagger}_{j\to i}$ (at 37 °C) (kcal/mol)	16.2 ± 11.7 $(16.1^{+4.1}_{-4.3})$	14.8 ± 3.5 $(11.5^{+22.8}_{-ND})$	7.0 ± 7.8 $(7.2^{+5.7}_{-7.1})$
$k_{i\to j}$(at 37 °C) (s^{-1})[d]	$9.3^{+5.2}_{-3.3}$	$0.4^{+0.3}_{-0.1}$	$1.0^{+0.2}_{-0.6}$
$k_{j\to i}$ (at 37 °C) (s^{-1})[d]	$118.6^{+65.3}_{-42.1}$	$(3.6^{+2.1}_{-1.3})$ x 10^3	$(9.9^{+17.1}_{-6.3})$ x 10^3

[a]PK: pseudoknot; pkHP1: hairpin 1 in the pseudoknot context; HP1: truncated hairpin with stem 1; U: fully unfolded state. *ND*: Error could not be determined. [b]Parameters are for the 3-state sequential model for VPK-2AP, with folding/unfolding via the dominant pathway that populates pkHP1. The two values reported for each quantity (with and without parenthesis) are from two different methods for obtaining the best fit parameters and their errors. For values on the top, the parameters and their errors were obtained from the weighted average and standard deviation, respectively, of all the fit parameters from 263 best fits that fell in the range of 1-1.5 times the lowest χ^2_ν obtained from 10,000 independent searches in parameter space, using the simulated annealing procedure as described in SI Methods 1.9. For values in parenthesis, the fit parameters and their errors were calculated as described in SI Methods 1.5. [c] Parameters are for the 2-state model of HP1-2AP. The two sets of values are as described above for VPK-2AP. In the parameters obtained from the simulated annealing procedure, parameters were averaged from 550 best fits out of 10,000 independent searches in parameter space. [d]The unfolding/folding rate coefficients at 37 °C ($k_{i\to j/j\to i}$) were calculated from the rate coefficients at T^0 ($k^0_{i\to j/j\to i}$) and the corresponding energy barriers ($\Delta H^{\ddagger}_{i\to j/j\to i}$); the uncertainties in these parameters were calculated from Eqs. S21–S24.

Table S4. Thermodynamic parameters of unlabeled HP2 and labeled HP2-pC at different salt concentrations[a]

	HP2 absorbance		HP2-pC absorbance		HP2-pC fluorescence	
Salt concentration (mM)	**ΔH (kcal/mol)**	**T_m (°C)**	**ΔH (kcal/mol)**	**T_m (°C)**	**ΔH (kcal/mol)**	**T_m (°C)**
50	$35.2^{+3.6}_{-3.4}$ ($32.4^{+1.4}_{-1.4}$)	$69.3^{+0.2}_{-0.2}$ ($69.4^{+0.2}_{-0.2}$)	$55.3^{+3.2}_{-4.1}$ ($60.1^{+6.8}_{-6.4}$)	$68.3^{+1.4}_{-1.4}$ ($71.9^{+0.6}_{-0.6}$)	$56.7^{+7.7}_{-6.2}$ ($36.6^{+2.2}_{-2.1}$)	$70.3^{+1.1}_{-1.2}$ ($70.6^{+0.5}_{-0.5}$)
100	$35.4^{+0.6}_{-0.6}$ ($42.1^{+1.1}_{-1.1}$)	$72.3^{+0.1}_{-0.1}$ ($72.4^{+0.1}_{-0.1}$)	$48.2^{+5.3}_{-5.0}$ ($53.4^{+3.6}_{-3.4}$)	$76.9^{+0.3}_{-0.3}$ ($76.9^{+0.4}_{-04}$)	$59.8^{+2.3}_{-2.2}$ ($41.5^{+1.0}_{-1.0}$)	$75.4^{+0.5}_{-0.5}$ ($74.0^{+0.4}_{-0.4}$)
200	$52.2^{+10.9}_{-9.0}$ ($45.3^{+1.4}_{-1.4}$)	$75.7^{+0.6}_{-0.6}$ ($76.2^{+0.2}_{-0.2}$)	$50.9^{+5.0}_{-4.7}$ ($51.9^{+3.2}_{-3.1}$)	$80.7^{+0.2}_{-0.2}$ ($80.3^{+0.3}_{-0.3}$)	$35.7^{+1.4}_{-1.4}$ ($27.5^{+1.2}_{-1.1}$)	$79.7^{+0.1}_{-0.1}$ ($80.6^{+3.1}_{-2.5}$)
500	$48.7^{+6.5}_{-6.0}$ ($48.2^{+0.7}_{-0.7}$)	$82.5^{+0.4}_{-0.4}$ ($82.4^{+0.1}_{-0.1}$)	$54.7^{+12.6}_{-11.0}$ ($51.2^{+4.3}_{-4.0}$)	$85.7^{+1.0}_{-0.6}$ ($86.0^{+0.4}_{-0.4}$)	$40.2^{+4.3}_{-4.3}$ ($38.0^{+3.9}_{-3.5}$)	$84.4^{+0.6}_{-0.6}$ ($87.3^{+5.3}_{-3.6}$)
1000	$48.9^{+3.7}_{-3.5}$ ($46.8^{+0.4}_{-0.4}$)	$85.3^{+0.5}_{-0.6}$ ($85.5^{+0.1}_{-0.1}$)	$58.2^{+10.3}_{-9.5}$ ($58.9^{+2.8}_{-2.7}$)	$87.7^{+1.0}_{-0.7}$ ($87.5^{+0.3}_{-0.3}$)	$48.9^{+3.7}_{-3.5}$ ($46.8^{+0.4}_{-0.4}$)	$85.3^{+0.5}_{-0.6}$ ($85.5^{+0.1}_{-0.1}$)

[a]Thermodynamic parameters are from fits to the absorbance or fluorescence melting profiles using a 2-state model, as described in SI Methods 1.3; parameters in parenthesis are from fits to the corresponding derivatives. The errors in the parameters were calculated as described in SI Methods 1.5. The melting temperatures reported in the text are the average of the values from the two different fits, rounded to the nearest integer.

Table S5. Thermodynamic parameters of VPK-2AP from fluorescence melting profiles at different salt concentrations[a]

		Salt concentration (mM)		
		50	**500**	**1000**
PK ⇔ pkHP1	T_m **(°C)**	$63.0^{+0.5}_{-0.5}$ ($52.8^{+1.8}_{-1.5}$)	$67.6^{+3.9}_{-3.6}$ ($67.5^{+4.4}_{-4.2}$)	$72.4^{+4.5}_{-4.7}$ ($74.3^{+4.8}_{-5.0}$)
	ΔH **(kcal/mol)**	$50.6^{+2.0}_{-2.5}$ ($40.6^{+1.2}_{-1.2}$)	$59.1^{+5.8}_{-5.9}$ ($55.0^{+5.2}_{-4.8}$)	$65.1^{+5.4}_{-5.1}$ ($44.2^{+5.7}_{-5.9}$)
pkHP1 ⇔ U	T_m **(°C)**	$85.0^{+0.5}_{-0.5}$ ($84.5^{+0.4}_{-0.5}$)	$93.6^{+1.0}_{-1.0}$ ($93.2^{+1.1}_{-1.1}$)	$94.8^{+0.9}_{-0.8}$ ($95.0^{+1.4}_{-1.3}$)
	ΔH **(kcal/mol)**	$67.9^{+2.8}_{-7.3}$ ($49.2^{+1.5}_{-1.3}$)	$50.3^{+1.6}_{-1.5}$ ($50.6^{+1.9}_{-2.0}$)	$45.6^{+2.1}_{-2.2}$ ($50.0^{+1.8}_{-1.8}$)
PK ⇔ pkHP2	T_m **(°C)**	------	$74.4^{+1.6}_{-1.6}$ ($73.0^{+1.7}_{-1.8}$)	$72.7^{+2.1}_{-1.8}$ ($77.2^{+1.9}_{-2.0}$)
	ΔH **(kcal/mol)**	------	$49.4^{+5.3}_{-4.7}$ ($47.5^{+5.5}_{-5.6}$)	$53.3^{+3.6}_{-4.1}$ ($40.7^{+5.3}_{-4.6}$)
pkHP2 ⇔ U	T_m **(°C)**	------	$83.1^{+1.0}_{-0.9}$ ($84.6^{+1.1}_{-1.1}$)	$89.5^{+1.1}_{-1.1}$ ($89.1^{+1.4}_{-1.5}$)
	ΔH **(kcal/mol)**	------	$60.0^{+3.3}_{-3.1}$ ($58.1^{+2.7}_{-2.5}$)	$57.9^{+3.4}_{-3.1}$ ($53.5^{+3.4}_{-3.4}$)

[a]The reported values are from fits to VPK-2AP fluorescence melting profiles using a 3-states model (for 50 mM) or a 4-states model (for 500 and 1000 mM) model, as described in SI Methods 1.3-1.4; parameters in parenthesis are from fits to the corresponding derivatives. The parameters in this Table are the average from two sets of fits: one in which the PK ⇔ pkHP1 transition temperature was constrained from simulation results, and the other in which the PK ⇔ pkHP2 transition temperature was constrained. For each set of fits, the errors in the parameters were obtained as described in SI Methods 1.5. The uncertainties in each parameter represent the compounded errors calculated from the two sets of fits as: $\sigma = \frac{\sqrt{\sigma_1^2+\sigma_2^2}}{2}$.

Table S6. Thermodynamic parameters of VPK-pC from fluorescence melting profiles at different salt concentrations[a]

		Salt concentration (mM)				
		50	**100**	**200**	**500**	**1000**
PK ⇔ pkHP1	T_m **(°C)**	$46.0^{+0.7}_{-0.7}$ ($46.0^{+0.4}_{-0.4}$)	$51.4^{+0.8}_{-0.9}$ ($53.6^{+3.0}_{-3.0}$)	$58.4^{+0.7}_{-0.8}$ ($62.8^{+4.4}_{-4.1}$)	$65.3^{+0.8}_{-0.9}$ ($69.4^{+3.8}_{-3.8}$)	$72.8^{+0.8}_{-0.8}$ ($73.5^{+3.3}_{-3.4}$)
	ΔH **(kcal/mol)**	$31.2^{+2.5}_{-3.4}$ ($27.0^{+1.5}_{-1.6}$)	$23.4^{+4.2}_{-4.6}$ ($16.9^{+6.2}_{-5.6}$)	$23.3^{+3.9}_{-2.7}$ ($14.4^{+5.7}_{-4.7}$)	$27.4^{+2.9}_{-3.1}$ ($17.3^{+4.6}_{-4.6}$)	$35.6^{+4.5}_{-5.6}$ ($16.2^{+6.5}_{-5.4}$)
pkHP1 ⇔ U	T_m **(°C)**	$79.0^{+0.5}_{-0.5}$ ($79.1^{+0.2}_{-0.2}$)	$81.0^{+0.7}_{-0.7}$ ($81.0^{+1.1}_{-1.1}$)	$85.0^{+1.3}_{-1.1}$ ($85.2^{+1.6}_{-1.6}$)	$87.9^{+0.9}_{-0.8}$ ($88.1^{+1.1}_{-1.1}$)	$89.0^{+0.6}_{-0.6}$ ($89.1^{+0.8}_{-0.8}$)
	ΔH **(kcal/mol)**	$40.0^{+2.3}_{-23}$ ($40.6^{+2.0}_{-1.8}$)	$55.3^{+2.9}_{-2.8}$ ($55.0^{+2.9}_{-2.8}$)	$48.5^{+4.4}_{-3.3}$ ($39.1^{+5.4}_{-4.2}$)	$43.0^{+2.4}_{-2.8}$ ($42.6^{+3.1}_{-3.1}$)	$45.0^{+1.8}_{-1.8}$ ($45.2^{+1.8}_{-1.8}$)
PK ⇔ pkHP2	T_m **(°C)**	------	$69.2^{+0.7}_{-0.8}$ ($71.7^{+0.9}_{-0.9}$)	$73.9^{+1.1}_{-1.3}$ ($76.4^{+1.5}_{-1.4}$)	$73.1^{+1.7}_{-1.6}$ ($78.5^{+1.3}_{-1.1}$)	$80.3^{+1.0}_{-1.0}$ ($83.5^{+1.2}_{-1.3}$)
	ΔH **(kcal/mol)**	------	$38.6^{+3.1}_{-3.5}$ ($31.8^{+2.4}_{-2.4}$)	$39.8^{+1.9}_{-3.3}$ ($27.0^{+4.1}_{-4.2}$)	$30.6^{+3.2}_{-2.9}$ ($20.1^{+5.1}_{-2.8}$)	$50.6^{+2.3}_{-5.0}$ ($31.4^{+3.3}_{-2.9}$)
pkHP2 ⇔ U	T_m **(°C)**	------	$74.2^{+0.7}_{-0.7}$ ($74.2^{+1.1}_{-1.2}$)	$78.4^{+1.6}_{-1.5}$ ($78.2^{+1.4}_{-1.8}$)	$83.2^{+0.7}_{-0.7}$ ($83.0^{+1.3}_{-1.3}$)	$84.1^{+0.9}_{-0.8}$ ($82.6^{+2.8}_{-3.0}$)
	ΔH **(kcal/mol)**	------	$40.0^{+3.7}_{-3.6}$ ($40.2^{+4.0}_{-3.8}$)	$31.5^{+5.5}_{-3.1}$ ($26.6^{+4.8}_{-5.1}$)	$39.7^{+2.8}_{-2.5}$ ($40.2^{+3.0}_{-3.2}$)	$30.0^{+4.0}_{-4.1}$ ($30.0^{+4.3}_{-4.3}$)

[a]Thermodynamic parameters are from fits to VPK-pC fluorescence melting profiles using a 3-state model (for 50 mM salt) or 4-state model (for 100, 200, 500 and 1000 mM salt), as described in SI Methods 1.3-1.4; parameters in parenthesis are from fits to the corresponding derivatives. The parameters in this Table are the average from two sets of fits: one in which the PK ⇔ pkHP1 transition temperature was constrained from simulation results, and the other in which the PK ⇔ pkHP2 transition temperature was constrained. For each set of fits, the errors in the parameters were obtained as described in SI Methods 1.5. The uncertainties in each parameter represent the compounded errors calculated from the two sets of fits as: $\sigma = \frac{\sqrt{\sigma_1^2+\sigma_2^2}}{2}$.

Table S7. Transition temperatures (in ^{o}C) between different macrostates in the 4-state parallel pathway model, from simulations (left) and experiments (right)[a]

Salt concentration (mM)	PK ⇔ pkHP1		pkHP1 ⇔ U		PK ⇔ pkHP2		pkHP2 ⇔ U	
50	47.2	$46.0^{+0.3}_{-0.3}$	84.3	$79.0^{+0.1}_{-0.1}$	64.9	------	70.6	------
100	53.1	$52.5^{+2.0}_{-2.0}$	85.6	$81.0^{+0.7}_{-0.7}$	70.7	$70.5^{+0.6}_{-0.6}$	70.7	$74.2^{+0.7}_{-0.7}$
200	60.4	$60.6^{+3.0}_{-2.7}$	86.5	$85.1^{+1.2}_{-1.1}$	74.5	$75.1^{+0.9}_{-1.0}$	74.5	$78.3^{+1.1}_{-1.2}$
500	66.7	$67.3^{+2.3}_{-2.3}$	87.6	$88.0^{+0.8}_{-0.7}$	78.0	$75.8^{+1.1}_{-1.0}$	78.0	$83.1^{+0.7}_{-0.7}$
1000	70.8	$73.1^{+2.2}_{-2.3}$	88.2	$89.1^{+0.5}_{-0.5}$	80.0	$81.9^{+0.8}_{-0.8}$	80.0	$83.4^{+1.5}_{-1.6}$

[a]The experimental values are the average of four sets of fits to the VPK-pC fluorescence melting profiles, as described in SI Methods 1.4 and shown in Figure S14: two from fits to the VPK-2AP melting profiles and two from fits to the derivatives, with either the PK ⇔ pkHP1 or the PK ⇔ pkHP2 transition temperature constrained from the simulation results. For each set of fits, the errors in the parameters were obtained as described in SI Methods 1.5. The uncertainties in the transition temperatures represent the compounded errors calculated from the four sets of fits as: $\sigma = \frac{\sqrt{\sigma_{m1}^2+\sigma_{m2}^2+\sigma_{d1}^2+\sigma_{d2}^2}}{4}$, where $\sigma_{m1,2}$ are the errors from the two fits to the melting profiles and $\sigma_{d1,2}$ are the errors from the two fits to the corresponding derivatives.

Table S8. Folding times at 37 °C from simulations

Pathway	**Through pkHP1**	**Through pkHP2**
τ (U → pkHP)[a] (at 37 °C)	70 μs	50 μs
τ (pkHP → PK)[a] (at 37 °C)	1.51 ms	110 μs

[a]PK: pseudoknot; pkHP: partially folded (hairpin) intermediate; U: fully unfolded state.

References

1. Bevington PR, Robinson DK (2003) *Data Reduction and Error Analysis for the Physical Sciences* (McGraw-Hill, New York, NY). Third Ed.
2. Kuznetsov S V., Kozlov AG, Lohman TM, Ansari A (2006) Microsecond dynamics of protein-DNA interactions: direct observation of the wrapping/unwrapping kinetics of single-stranded DNA around the E. coli SSB tetramer. *J Mol Biol* 359:55–65.
3. Kuznetsov S V., Ren C-C, Woodson SA, Ansari A (2008) Loop dependence of the stability and dynamics of nucleic acid hairpins. *Nucleic Acids Res* 36:1098–1112.
4. Wray WO, Aida T, Dyer RB (2002) Photoacoustic cavitation and heat transfer effects in the laser-induced temperature jump in water. *Appl Phys B Lasers Opt* 74:57–66.
5. Vivas P, Kuznetsov S V., Ansari A (2008) New insights into the transition pathway from nonspecific to specific complex of DNA with Escherichia coli integration host factor. *J Phys Chem B* 112:5997–6007.
6. Kuznetsov S V., Ansari A (2012) A kinetic zipper model with intrachain interactions applied to nucleic acid hairpin folding kinetics. *Biophys J* 102:101–111.
7. Kirkpatrick S, Gelatt CD, Vecchi MP (1983) Optimization by Simulated Annealing. *Science* 220:671–680.
8. Press WH, Flannery BP, Teukolsky SA (1986) *Numerical Recipes: The Art of Scientific Computing* (Cambridge University Press, Cambridge).
9. Ansari A, Jones CM, Henry ER, Hofrichter J, Eaton WA (1994) Conformational Relaxation and Ligand Binding in Myoglobin. *Biochemistry* 33:5128–5145.
10. Denesyuk NA, Thirumalai D (2013) Coarse-grained model for predicting RNA folding thermodynamics. *J Phys Chem B* 117:4901–4911.
11. Hori N, Denesyuk NA, Thirumalai D (2016) Salt effects on the thermodynamics of a frameshifting RNA pseudoknot under tension. *J Mol Biol* 428:2847–2859.
12. Honeycutt JD, Thirumalai D (1992) The nature of folded states of globular proteins. *Biopolymers* 32:695–709.
13. Sugita Y, Okamoto Y (1999) Replica-exchange molecular dynamics method for protein folding. *Chem Phys Lett* 314:141–151.

14. Hyeon C, Thirumalai D (2008) Multiple probes are required to explore and control the rugged energy landscape of RNA hairpins. *J Am Chem Soc* 130:1538–1539.
15. Cho SS, Pincus DL, Thirumalai D (2009) Assembly mechanisms of RNA pseudoknots are determined by the stabilities of constituent secondary structures. *Proc Natl Acad Sci U S A* 106:17349–17354.